HU-EP-17/04
TTK-17-03

Production of heavy Higgs bosons and decay into top quarks at the LHC. II: Top-quark polarization and spin correlation effects

W. Bernreuther [a,1], **P. Galler** [b,2], **Z.-G. Si** [c,3] **and P. Uwer** [b,4]

[a]Institut für Theoretische Teilchenphysik und Kosmologie, RWTH Aachen University, 52056 Aachen, Germany
[b]Institut für Physik, Humboldt-Universität zu Berlin, 12489 Berlin, Germany
[c]School of Physics, Shandong University, Jinan, Shandong 250100, China

Abstract

We analyze, within several parameter scenarios of type-II two-Higgs doublet extensions of the standard model, the impact of heavy neutral Higgs-boson resonances on top-quark pair production and their subsequent decay to dileptonic final states at the LHC (13 TeV). In particular, we investigate the effects of heavy Higgs bosons on top-spin observables, that is, the longitudinal top-quark polarization and top-quark spin correlations. We take into account NLO QCD as well as weak interaction corrections and show that top-spin observables, if evaluated in judiciously chosen top-quark pair invariant mass bins, can significantly enhance the sensitivity to heavy Higgs resonances in top-quark pair events.

Keywords: hadron collider physics, Higgs boson, top quark, QCD corrections, spin effects, new physics

[1] breuther@physik.rwth-aachen.de
[2] galler@physik.hu-berlin.de
[3] zgsi@sdu.edu.cn
[4] peter.uwer@physik.hu-berlin.de

1. Introduction

One of the central issues of present and future research at the Large Hadron Collider (LHC) is the search for new, in particular heavy (pseudo-)scalar bosons with masses below or around 1 TeV. The existence of additional spin-zero resonances besides the 125 GeV Higgs resonance [1,2] is theoretically well motivated [3,4]. Experimental searches were negative so far (cf. for instance [5]), but are by far not exhaustive and will continue with increased effort at the run II of the LHC at 13 TeV center-of-mass energy.

A possibility that has received increased experimental attention recently [6–9] is the existence of one or several neutral Higgs bosons with masses above the top-antitop quark ($t\bar{t}$) production threshold that strongly couple to top quarks but have suppressed couplings to the weak gauge bosons and to d-type quarks and charged leptons. The search for such a Higgs boson (or Higgs bosons) in $t\bar{t}$ production is difficult because one expects that its line shape in the $t\bar{t}$ invariant mass spectrum is not a distinctive resonance bump but is significantly distorted which is caused by the interference of the signal and the nonresonant $t\bar{t}$ background amplitudes. As far as experimental investigations are concerned, this interference effect was taken into account only in the recent data analysis [9] of the ATLAS experiment.

Future experimental explorations of this search channel aiming at an increased sensitivity to such type of Higgs bosons require for their interpretation theoretical investigations beyond leading-order (LO) QCD. In [10] we have investigated, within the type-II two-Higgs-doublet extension (2HDM) of the standard model (SM), the production of heavy neutral Higgs bosons and their decay to $t\bar{t}$ pairs including signal-background interference at next-to-leading-order (NLO) in the QCD coupling. The NLO QCD corrections to Higgs production and signal-background interference were computed in the heavy top-quark mass limit with an effective K-factor rescaling. The primary aim of this exploration was to analyze how the QCD corrections affect the distortions of the $t\bar{t}$ invariant mass spectrum and of other distributions in the resonance region. Another NLO QCD analysis of heavy Higgs-boson production in the $t\bar{t}$ channel including interference with the $t\bar{t}$ background was recently presented in [11].

In this paper we extend our investigations of [10] by taking the t and $\bar{t}$ polarization and $t\bar{t}$ spin correlations fully into account at NLO QCD. We consider, again within the type-II 2HDM, the production of heavy neutral Higgs bosons and their decay to $t\bar{t}$ with subsequent decay of $t\bar{t}$ to dileptonic final states, including signal-background interference and the irreducible nonresonant $t\bar{t}$ background at NLO QCD. In our computation of the nonresonant $t\bar{t}$ background the mixed QCD-weak interaction corrections are also included. Our goal is to analyze the sensitivity of top-spin observables to heavy Higgs resonances. We explore lepton angular distributions and dileptonic angular correlations [12, 13] that are induced by t and $\bar{t}$ polarizations and $t\bar{t}$ spin correlations. We compute these observables in appropriately chosen $t\bar{t}$ invariant mass windows in the standard model and in the presence of heavy Higgs resonances. Heavy Higgs-boson effects on $t\bar{t}$ spin correlations were previously investigated at LO QCD in [14–18].

The paper is organized as follows. In Sec. 2 we briefly recapitulate the salient features of the

type-II 2HDM with and without Higgs-sector CP violation that are relevant for our analysis and define four parameter scenarios. In Sec. 3 we introduce spin dependent observables. In Sec. 4 we show in analogy to what has been done in Ref. [10] results for the invariant mass distribution of the $t\bar{t}$ pair at the level of the intermediate top quarks. These results are then compared, as far as the sensitivity to heavy Higgs bosons is concerned, with predictions for spin dependent observables in dileptonic $t\bar{t}$ events. All results are shown for the LHC operating at 13 TeV and are presented both for selected $M_{t\bar{t}}$ bins and inclusively in $M_{t\bar{t}}$. We conclude in Sec. 5.

2. Parameter scenarios for the type-II two-Higgs-doublet model

For definiteness we choose, as in [10], the type-II two-Higgs-doublet model for describing both the 125 GeV Higgs resonance and additional neutral heavy Higgs bosons in a consistent field-theoretic and phenomenologically viable framework. We recall that in 2HDMs the SM field content is extended by an additional Higgs doublet. In the type-II 2HDM the Higgs doublet Φ_1 is coupled to right-chiral down-type quarks and charged leptons, while Φ_2 is coupled to right-chiral up-type quarks only. By construction, flavor-changing neutral currents are absent at tree level.

Because we are interested in heavy Higgs bosons of different CP nature we consider two variants of the type-II 2HDM: one where the tree-level Higgs potential $V(\Phi_1, \Phi_2)$ is CP-violating and, as a special case, the model where $V(\Phi_1, \Phi_2)$ is CP-invariant. We denote the three physical neutral Higgs mass eigenstates by ϕ_j, $j = 1, 2, 3$. Using the unitary gauge they are related to the two CP-even and the CP-odd states $\varphi_{1,2}$ and A, respectively, by an orthogonal transformation:

$$(\phi_1, \phi_2, \phi_3)^T = R(\varphi_1, \varphi_2, A)^T \,, \tag{1}$$

where R is a real orthogonal matrix that is parametrized by three mixing angles α_i. We use the parametrization of R given in [10]. The masses of the three neutral Higgs bosons and of the charged Higgs boson $H^\pm$ of the model are denoted by m_j ($j = 1, 2, 3$) and by m_+, respectively. The parameter $\tan\beta = v_2/v_1$ is the ratio of the vacuum expectation values of the two Higgs doublet fields with $v = \sqrt{v_1^2 + v_2^2} = 246$ GeV. In the case of Higgs sector CP violation we choose, as in [10],

$$m_1, m_2, m_3, m_+, \alpha_1, \alpha_2, \alpha_3, \tan\beta, v, \tag{2}$$

to belong to the set of independent parameters of the model, while in the case where $V(\Phi_1, \Phi_2)$ is CP-invariant we choose

$$m_1, m_2, m_3, m_+, \alpha_1, \tan\beta, v \,. \tag{3}$$

In this case the matrix R is block-diagonal with $R_{13} = R_{23} = R_{31} = R_{32} = 0$ and $R_{33} = 1$, and the neutral Higgs mass eigenstates consist of two CP-even and a CP-odd state which are often denoted by $\phi_1 = h$, $\phi_2 = H$, and $\phi_3 = A$. In the more general case of Higgs sector CP violation the ϕ_j are CP mixtures.

The interactions of the ϕ_j with quarks and charged leptons $f = q, \ell$ and with weak gauge boson pairs are given by

$$\mathcal{L}_1 = -\frac{m_f}{v}\left(a_{jf}\bar{f}f - b_{jf}\bar{f}i\gamma_5 f\right)\phi_j + f_{jVV}\phi_j\left(\frac{2m_W^2}{v}W_\mu^- W^{+\mu} + \frac{m_Z^2}{v}Z_\mu Z^\mu\right), \tag{4}$$

where a sum over f and $j = 1,2,3$ is understood. The reduced scalar and pseudoscalar Yukawa couplings a_{jf} and b_{jf} and the reduced couplings f_{jVV} depend on the values of $\tan\beta$ and on the elements R_{ij} of the Higgs mixing matrix. They are listed in Tab. 1 for the type-II model. We recall that the reduced gauge-boson couplings obey the sum rule $\sum_j f_{jVV}^2 = 1$. For computing the widths of the heavy Higgs bosons below we need also the triple Higgs and the $Z\phi_i\phi_j$ interactions. They are given, for instance, in [10, 19, 20]. We identify the 125 GeV Higgs res-

Table 1: Reduced couplings to quarks, leptons and gauge bosons of the neutral Higgs bosons ϕ_j of the type-II 2HDM defined in Eq. (4). The labels t, b, and τ refer to u-type, d-type quarks, and charged leptons.

a_{jt}	$a_{jb} = a_{j\tau}$	b_{jt}	$b_{jb} = b_{j\tau}$	f_{jVV}
$R_{j2}/\sin\beta$	$R_{j1}/\cos\beta$	$R_{j3}\cot\beta$	$R_{j3}\tan\beta$	$\cos\beta R_{j1} + \sin\beta R_{j2}$

onance with ϕ_1 and assume that the mass of both ϕ_2 and ϕ_3 is larger than twice the top-quark mass, $m_{2,3} > 2m_t$. Moreover, we assume that the mass of the charged Higgs boson H^+ is of the order of $\max(m_2, m_3)$, so that the two-body decays $\phi_{2,3} \to W^\pm H^\mp$ cannot take place. The ATLAS and CMS results [21] on the 125 GeV Higgs boson imply that its interactions with the third-generation fermions and gauge bosons are SM-like. This constraint is taken into account in the 2HDM parameter scenarios defined below.

As already emphasized in the introduction our aim is to investigate the sensitivity of top-spin observables to heavy Higgs-bosons and, in particular, whether suitable observables allow to discriminate between a scalar, pseudoscalar, and a CP mixture. For this purpose we choose three parameter sets, which we call set 1a, 1b, and 1c, where the masses of the two heavy neutral Higgs bosons are put to 400 GeV and 900 GeV. Sets 1a and 1b are associated with a CP-invariant Higgs potential. In set 1a we assign the quantum numbers CP =+1 and CP =-1 to the 400 GeV and 900 GeV Higgs boson, respectively, and vice versa in set 1b. Set 1c is associated with a CP-violating Higgs potential and the neutral Higgs bosons are chosen to be CP mixtures. In addition we investigate the case where the two heavy neutral Higgs bosons are nearly degenerate with masses that are substantially larger than $2m_t$. This is exemplified with a parameter set called set 2 below.

We determine the total widths of the heavy neutral Higgs bosons ϕ_2 and ϕ_3 for the four parameter sets specified below, by computing the sum of the largest two-body decay rates. We include the NLO QCD corrections to the partial decay rates of $\phi_j \to q\bar{q}$ and $\phi_j \to gg$ using the formulas of [22, 23] and [24], respectively. In these computations we use the input parameters and the scale choice as described in Sec. 4.1. We checked, where possible, our results with the computer codes of [25] and [26]. For the parameter sets below, the total width Γ_1 of $\phi_1(125\text{ GeV})$ is of the order of 4 MeV. It plays no role in the computations of Sec. 4.

Scenarios 1a and 1b

We consider the type-II model with a CP-conserving Higgs potential. We choose both for the parameter set 1a and 1b:

$$\tan\beta = 1\,, \quad \alpha_1 = \beta\,, \quad \alpha_2 = \alpha_3 = 0\,, \quad m_1 = 125\,\text{GeV}\,, \quad m_+ > 820\,\text{GeV}\,. \tag{5}$$

With this choice of the Higgs mixing angles and our convention for R [10] the states ϕ_1 and ϕ_2 are CP-even while ϕ_3 is CP-odd, as can be seen from the resulting Yukawa couplings given in Tab. 2. The masses of ϕ_2 and ϕ_3 are set to the values

$$\begin{aligned} &\text{scenario 1a:} \quad m_2 = 400\,\text{GeV}\,, \quad m_3 = 900\,\text{GeV}\,, \\ &\text{scenario 1b:} \quad m_2 = 900\,\text{GeV}\,, \quad m_3 = 400\,\text{GeV}\,. \end{aligned} \tag{6}$$

Thus in scenario 1a the lighter of the two heavy states is chosen to be a pure scalar while in scenario 1b it is a pseudoscalar.
We compute the largest two-body decay rates of ϕ_2 and ϕ_3 and determine their total widths by adding up these rates. The results are listed in Tab. 3 and Tab. 4 for scenario 1a and 1b, respectively. The uncertainties result from varying the renormalization scale as described below Eq. (33). The partial decay widths of $\phi_j \to f\bar{f}$ ($f \neq t$), $\phi_j \to \gamma\gamma$, and $\phi_j \to Z\gamma$ are a few $\times 10^{-3}$ GeV or smaller[1] and are neglected in the total widths Γ_2, Γ_3. Moreover, to lowest order in the non-QCD couplings the partial decay rates for $\phi_i \to VV$, $\phi_i \to \phi_1 Z$ and $\phi_i \to \phi_1\phi_1$ ($i = 2,3$) are zero for our choice of parameters.

Table 2: Values of the reduced couplings to fermions and vector bosons $V = W, Z$ of the neutral Higgs bosons ϕ_j in scenarios 1a, 1b and 2.

	a_{jt}	$a_{jb} = a_{j\tau}$	b_{jt}	$b_{jb} = b_{j\tau}$	f_{jVV}
ϕ_1	1	1	0	0	1
ϕ_2	1	-1	0	0	0
ϕ_3	0	0	1	1	0

Scenario 1c

Here we consider the type-II model with a CP-violating Higgs potential and choose

$$\tan\beta = 1\,, \quad \alpha_1 = \beta\,, \quad \alpha_2 = \frac{\pi}{15}\,, \quad \alpha_3 = \frac{\pi}{4}\,, \quad m_1 = 125\,\text{GeV}\,, \quad m_+ > 820\,\text{GeV}\,. \tag{7}$$

[1] The partial decay width of $\phi_j \to \gamma\gamma$ ($j = 2,3$) in these parameter scenarios and in the scenarios 1c and 2 below is $\lesssim 3 \times 10^{-4}$ GeV.

Table 3: Dominant partial decay widths and the total width of the CP-even and CP-odd Higgs boson ϕ_2 and ϕ_3, respectively, in scenario 1a.

decay mode	Γ_2 [GeV]	Γ_3 [GeV]
$\phi_i \to t\bar{t}$	$3.97^{+0.10}_{-0.08}$	$45.43^{-0.36}_{+0.30}$
$\phi_i \to \phi_2 Z$	0	116.85
$\phi_i \to gg$	$0.017^{+0.003}_{-0.002}$	$0.107^{-0.0003}_{-0.0036}$
total	$3.99^{+0.10}_{-0.08}$	$162.39^{-0.36}_{+0.30}$

Table 4: Dominant partial decay widths and the total width of the CP-odd and CP-even Higgs boson ϕ_2 and ϕ_3, respectively, in scenario 1b.

decay mode	Γ_2 [GeV]	Γ_3 [GeV]
$\phi_i \to t\bar{t}$	$39.85^{-0.20}_{+0.17}$	$15.09^{+0.31}_{-0.26}$
$\phi_i \to \phi_3 Z$	116.85	0
$\phi_i \to gg$	$0.068^{+0.004}_{-0.005}$	$0.051^{+0.009}_{-0.007}$
total	$156.76^{-0.19}_{+0.16}$	$15.14^{+0.32}_{-0.27}$

With this choice of the Higgs mixing angles the states ϕ_j are CP mixtures. Their reduced Yukawa couplings and reduced couplings to W,Z are given in Tab. 5. The masses of ϕ_2 and ϕ_3 are set to the values

$$\text{scenario 1c:} \quad m_2 = 400\,\text{GeV}\,, \quad m_3 = 900\,\text{GeV}\,. \tag{8}$$

The partial widths of the major decay modes of ϕ_2 and ϕ_3 and their total widths are listed in Tab. 6. Decay modes whose width is smaller than a few $\times 10^{-3}$ GeV are not listed. The given uncertainties result from the scale variations as defined below Eq. (33) in Sec. 4.1.

Table 5: Values of the reduced couplings to fermions and vector bosons $V = W,Z$ of the neutral Higgs bosons ϕ_j in scenario 1c.

	a_{jt}	$a_{jb} = a_{j\tau}$	b_{jt}	$b_{jb} = b_{j\tau}$	f_{jVV}
ϕ_1	0.978	0.978	0.208	0.208	0.978
ϕ_2	0.560	-0.854	0.692	0.692	-0.147
ϕ_3	-0.854	0.560	0.692	0.692	-0.147

Table 6: Dominant partial decay widths and the total width of the CP mixtures ϕ_2 and ϕ_3 in scenario 1c.

decay mode	Γ_2 [GeV]	Γ_3 [GeV]
$\phi_i \to t\bar{t}$	$8.47^{+0.18}_{-0.15}$	$50.80^{-0.32}_{+0.27}$
$\phi_i \to VV$	0.52	7.37
$\phi_i \to \phi_1 Z$	0.27	4.73
$\phi_i \to \phi_2 Z$	0	111.80
$\phi_i \to \phi_1\phi_1$	3.20	6.14
$\phi_i \to \phi_1\phi_2$	0	4.00
$\phi_i \to \phi_2\phi_2$	0	11.81
$\phi_i \to gg$	$0.030^{+0.005}_{-0.004}$	$0.100^{+0.003}_{-0.005}$
total	$12.49^{+0.19}_{-0.15}$	$184.95^{-0.32}_{+0.26}$

Scenario 2

We choose again a CP-conserving neutral Higgs sector scenario with the same values of m_1, m_+, $\tan\beta$, and Higgs mixing angles α_i as in scenarios 1a,b—cf. Eq. (5). Thus, the reduced couplings of the ϕ_j given in Tab. 2 apply also to this scenario. The states ϕ_1 and ϕ_2 are CP-even while ϕ_3 is CP-odd. The masses of the two heavy neutral Higgs bosons are set to the values

$$\text{scenario 2:} \quad m_2 = 766\,\text{GeV}\,, \quad m_3 = 750\,\text{GeV}\,. \tag{9}$$

The total decay widths of the nearly mass-degenerate scalar and pseudoscalar ϕ_2 and ϕ_3 are essentially determined by the decay of these states to $t\bar{t}$, cf. Tab. 7. Again, decay modes whose width is smaller than a few $\times 10^{-3}$ GeV are not exhibited in this table.

Table 7: Dominant partial decay widths and the total width of the CP-even and CP-odd Higgs boson ϕ_2 and ϕ_3, respectively, in scenario 2.

decay mode	Γ_2 [GeV]	Γ_3 [GeV]
$\phi_i \to t\bar{t}$	$31.92^{-0.03}_{+0.02}$	$37.94^{-0.14}_{+0.12}$
$\phi_i \to gg$	$0.055^{+0.005}_{-0.005}$	$0.087^{+0.006}_{-0.006}$
total	$31.97^{-0.02}_{+0.02}$	$38.03^{-0.13}_{+0.11}$

Experimental constraints

The Yukawa couplings and couplings to the weak gauge bosons that are assigned to the 125 GeV resonance in the above parameter scenarios are in accord with the constraints from the LHC [21]. The strongest direct constraints on heavy neutral Higgs bosons with strong couplings to top quarks were recently reported by the ATLAS experiment [9]. In this report the 2HDM parameter region $\tan\beta < 0.45$ ($\tan\beta < 0.85$) was excluded at 95% confidence level for a CP-even (CP-odd) Higgs boson H (A) with a mass of 500 GeV. This analysis is based on $t\bar{t}$ events that decay to leptons plus jets recorded at the LHC (8 TeV). The result supersedes previous bounds by ATLAS [7] and CMS [6, 8]. Our parameter scenarios 1a,b,c above are not in direct conflict with the bounds of [9] because our choice $\tan\beta = 1$ implies weaker top-Yukawa couplings of H and A than those excluded in [9]: In the case of H (A) the squared top-Yukawa coupling that enters the cross section for $gg \to \phi \to t\bar{t}$ is reduced by a factor 0.20 (0.72). This suggests that a Higgs boson with a mass of 400 GeV and top-Yukawa coupling strength as chosen in the scenarios 1a,b,c is not yet excluded. We emphasize that the analysis below does not crucially depend on the fact that we have chosen the mass of the lighter of the two heavy states to be 400 GeV. The sole purpose of these parameter choices is to illustrate

with these examples the sensitivity of top-spin observables to heavy Higgs resonances.
The charged Higgs boson $H^\pm$ of the 2HDM plays no decisive role in our analysis below. Our assumption $m_+ > 820$ GeV is in accord with the non-observation of $H^\pm$ in direct searches at the LHC and with the bounds derived from B physics data [27–29].

The LHC data on the 125 GeV Higgs boson constrain CP-violating top-Higgs couplings to some extent, see for instance [30]. A direct search for CP violation in semileptonic $t\bar{t}$ events at the LHC(8 TeV) was recently reported by the CMS experiment in [31]. The set of spin observables recently measured by the ATLAS experiment in dileptonic $t\bar{t}$ events at 8 TeV [32] include CP-odd observables and these measurements provide also direct bounds on CP violation in $t\bar{t}$ production. Our parameter scenario 1c is in accord with the constraints from these analyses. Stronger, albeit indirect constraints are obtained from low-energy data [19,33–35], in particular from the experimental upper limits on the electric dipole moments (EDMs) of the neutron [36] and the electron [37]. In the parameter scenario 1c the heavy Higgs bosons have only a minor impact on these EDMs. The major contribution results from ϕ_1 exchange. The Yukawa and gauge couplings of ϕ_1 given in Tab. 5 lie within the allowed parameter ranges derived in [19, 35].

3. Spin dependent observables

In the following we study the impact of heavy Higgs bosons on the (anti) top-quark polarization and top-antitop spin correlations, taking NLO QCD corrections into account. We follow Ref. [13] where a complete set of observables sufficient to constrain the spin density matrix at the level of stable top quarks has been presented. As in Ref. [13] we analyze the angular distributions of the (anti-)top-quark decay products. More specifically, we consider dileptonic $t\bar{t}$ events

$$pp \longrightarrow t + \bar{t} + X \longrightarrow \ell^+ \, \ell'^- + \text{jets} + E_T^{\text{miss}}, \quad \ell, \, \ell' = e, \mu, \tag{10}$$

and define four dileptonic angular correlations that correspond, at the level of the intermediate t and $\bar{t}$ quarks, to P- and CP-even $t\bar{t}$ spin correlations. In addition, we consider for the reactions (10) also a P-and CP-odd triple correlation and a lepton angular distribution that corresponds to the longitudinal top-quark polarization. Moreover, we analyze the correlation of the azimuthal angles of the charged leptons and investigate its sensitivity to the CP nature of the heavy Higgs bosons.

3.1. Observables sensitive to top-antitop spin correlations

We consider for (10) the following normalized differential distribution of the outgoing leptons:

$$\frac{1}{\sigma} \frac{d^2\sigma}{d\cos\theta_+ \, d\cos\theta_-} = \frac{1}{4} \left(1 + B_1 \cos(\theta_+) + B_2 \cos(\theta_-) - C \cos(\theta_+) \cos(\theta_-)\right), \tag{11}$$

where θ_+ (θ_-) denotes the angle between the direction of flight $\hat{\boldsymbol{\ell}}_+$ ($\hat{\boldsymbol{\ell}}_-$) of the positively (negatively) charged lepton in the (anti-)top-quark rest frame[2] and a reference axis $\hat{\mathbf{a}}$ ($\hat{\mathbf{b}}$) to be defined below ($\theta_+ = \angle(\hat{\boldsymbol{\ell}}_+, \hat{\mathbf{a}})$, $\theta_- = \angle(\hat{\boldsymbol{\ell}}_-, \hat{\mathbf{b}})$). We assume that the top-quarks decay dominantly via the SM decay $t \to W^+ b$ ($\bar{t} \to W^- \bar{b}$) with W-boson decaying further into a lepton neutrino pair. The coefficients B_1, B_2 and C depend on the chosen reference axes $\hat{\mathbf{a}}$ and $\hat{\mathbf{b}}$. If no acceptance cuts are applied, C is related to the double spin asymmetry at the level of the intermediate top quarks:

$$C_{\mathrm{ab}} \equiv C(\hat{\mathbf{a}}, \hat{\mathbf{b}}) = \kappa_\ell^2 \frac{\sigma_{t\bar{t}}(\uparrow\uparrow) + \sigma_{t\bar{t}}(\downarrow\downarrow) - \sigma_{t\bar{t}}(\uparrow\downarrow) - \sigma_{t\bar{t}}(\downarrow\uparrow)}{\sigma_{t\bar{t}}(\uparrow\uparrow) + \sigma_{t\bar{t}}(\downarrow\downarrow) + \sigma_{t\bar{t}}(\uparrow\downarrow) + \sigma_{t\bar{t}}(\downarrow\uparrow)}. \tag{12}$$

$\sigma_{t\bar{t}}$ denotes the cross section for top-quark pair production. The first (second) arrow refers to the spin state of the t ($\bar{t}$) quark with respect to the axis $\hat{\mathbf{a}}$ ($\hat{\mathbf{b}}$). The prefactor κ_ℓ^2 is due to the spin analyzer quality of the decay products. In the conventions used here

$$\kappa_\ell = \kappa_{\ell^+} = \kappa_{\ell^-}.$$

At NLO QCD its value is $\kappa_\ell = 1 - 0.015\alpha_s$ [38]. Following Ref. [13] we use the beam direction $\hat{\mathbf{p}} = (0, 0, 1)$ and the direction of flight of the top-quark $\hat{\mathbf{k}}$ in the $t\bar{t}$ zero-momentum frame (ZMF) to construct an orthonormal basis:

$$\{\hat{\mathbf{k}}, \hat{\mathbf{n}}, \hat{\mathbf{r}}\}: \quad \hat{\mathbf{r}} = \frac{1}{r}(\hat{\mathbf{p}} - y\hat{\mathbf{k}}), \quad \hat{\mathbf{n}} = \frac{1}{r}(\hat{\mathbf{p}} \times \hat{\mathbf{k}}), \tag{13}$$

with

$$y = \hat{\mathbf{p}} \cdot \hat{\mathbf{k}}, \quad r = \sqrt{1 - y^2}.$$

Using the orthonormal basis $\{\hat{\mathbf{k}}, \hat{\mathbf{n}}, \hat{\mathbf{r}}\}$ the reference axes $\hat{\mathbf{a}}$ and $\hat{\mathbf{b}}$ are defined in Tab. 8. The factor sign(y) takes the Bose symmetry of the initial gg state into account. Using the different

Table 8: Choice of reference axes. The unit vectors $\hat{\mathbf{n}}$, $\hat{\mathbf{r}}$ and the variable y are defined in Eq. (13). The factors sign(y) are required because of the Bose symmetry of the initial gg state.

	Label	$\hat{\mathbf{a}}$	$\hat{\mathbf{b}}$
transverse	n	sign(y) $\hat{\mathbf{n}}$	$-$sign(y) $\hat{\mathbf{n}}$
r axis	r	sign(y) $\hat{\mathbf{r}}$	$-$sign(y) $\hat{\mathbf{r}}$
helicity	k	$\hat{\mathbf{k}}$	$-\hat{\mathbf{k}}$

reference axes as shown in Tab. 8 nine different correlations $C(\hat{\mathbf{a}}, \hat{\mathbf{b}})$ can be defined. As far as P- and CP-even correlations are concerned we restrict ourselves to the diagonal correlations

$$C_{\mathrm{kk}},\ C_{\mathrm{nn}},\ \text{and}\ C_{\mathrm{rr}}.$$

[2]The respective rest frames are reached through a rotation-free boost from the $t\bar{t}$ zero-momentum frame.

These correlations are sensitive to the P- and CP-even contributions of the spin density matrix, do not require absorptive parts, and receive Higgs-boson contributions at leading order. Since the choice $\hat{\mathbf{a}} = \hat{\mathbf{k}}$ ($\hat{\mathbf{b}} = -\hat{\mathbf{k}}$) is equivalent to the quantization axis in the helicity basis, C_{kk} is often abbreviated in the literature as C_{hel}. In the following we adopt this notation and use C_{hel} instead of C_{kk}. Instead of measuring the double differential distribution as given in Eq. (11) the coefficient C can also be determined from the expectation value of $\cos(\theta_+)\cos(\theta_-)$:

$$\langle \cos(\theta_+)\cos(\theta_-)\rangle = -\frac{1}{9}C. \tag{14}$$

As pointed out in Ref. [13] the correlations $C_{\mathrm{hel}}, C_{\mathrm{nn}}$, and C_{rr} are related to the opening angle distribution

$$\frac{1}{\sigma}\frac{d\sigma}{d\cos\varphi} = \frac{1}{2}(1 - D\cos\varphi), \tag{15}$$

where the angle φ is defined by $\varphi = \sphericalangle(\hat{\boldsymbol{\ell}}_+, \hat{\boldsymbol{\ell}}_-)$. Since the vectors $\{\hat{\mathbf{k}}, \hat{\mathbf{n}}, \hat{\mathbf{r}}\}$ form an orthonormal basis the relation

$$D = -\frac{1}{3}(C_{\mathrm{hel}} + C_{\mathrm{nn}} + C_{\mathrm{rr}}) \tag{16}$$

holds. Eq. (16) may be used to cross check results. D can also be determined from the expectation value of $\cos\varphi$:

$$D = -3\langle\cos(\varphi)\rangle. \tag{17}$$

For completeness we note that both C_{ab} and D are related to expectation values of spin observables at the level of the intermediate top quarks:

$$C_{\mathrm{ab}} = \kappa_\ell^2 4\langle(\mathbf{S}_t \cdot \hat{\mathbf{a}})(\mathbf{S}_{\bar{t}} \cdot \hat{\mathbf{b}})\rangle, \tag{18}$$

$$D = \kappa_\ell^2 \frac{4}{3}\langle(\mathbf{S}_t \cdot \mathbf{S}_{\bar{t}})\rangle, \tag{19}$$

where $\mathbf{S}_t$ ($\mathbf{S}_{\bar{t}}$) denotes the (anti-)top-quark spin operator.

3.2. Observables sensitive to top-quark and antiquark polarization

Integrating out the angle of the positively/negatively charged lepton in Eq. (11) leads to a single differential distribution:

$$\frac{1}{\sigma}\frac{d\sigma}{d\cos\theta_\pm} = \frac{1}{2}(1 + B_{1,2}\cos(\theta_\pm)). \tag{20}$$

The coefficient B_1 (B_2) is related to the polarization of the intermediate (anti-)top-quark:

$$B_1(\hat{\mathbf{a}}) = \kappa_\ell\langle 2\mathbf{S}_t \cdot \hat{\mathbf{a}}\rangle, \quad B_2(\hat{\mathbf{b}}) = -\kappa_\ell\langle 2\mathbf{S}_{\bar{t}} \cdot \hat{\mathbf{b}}\rangle. \tag{21}$$

(The polarization is defined as twice the expectation value of the spin operator: $\mathbf{P}_t = 2\langle\mathbf{S}_t\rangle$.) For $\hat{\mathbf{a}} = \hat{\mathbf{k}}$ ($\hat{\mathbf{b}} = -\hat{\mathbf{k}}$) the coefficient B_1 (B_2) is a measure for the longitudinal polarization of the intermediate (anti-)top-quark. Note that a non-vanishing

$$B_t = B_1(\hat{\mathbf{k}}), \quad B_{\bar{t}} = B_2(-\hat{\mathbf{k}}) \tag{22}$$

requires a parity violating interaction. As a consequence, within the SM only the parity-violating weak interactions generate a small non-zero coefficient $B_1(\hat{\mathbf{k}})$ of less than 1 %. Similar to D the coefficients $B_{1,2}$ are related to expectation values of the respective angles:

$$B_{1,2} = 3\langle \cos\theta_{\pm} \rangle. \tag{23}$$

We note that the single differential distributions can also be studied for top-quark pairs decaying semi-leptonically. If no acceptance cuts are applied, the coefficient B_1 (B_2) parametrizing the distribution of the positively (negatively) charged lepton is the same in both channels.

3.3. Triple correlation

In addition to the aforementioned observables we analyze the P- and CP-odd triple correlation:

$$O_{CP} = (\hat{\boldsymbol{\ell}}_+ \times \hat{\boldsymbol{\ell}}_-) \cdot \hat{\mathbf{k}}. \tag{24}$$

The observable O_{CP} is sensitive to P- and CP-odd (dispersive) new physics contributions. Within the scenarios considered here only scenario 1c leads to a non-zero expectation value. As discussed in Ref. [13] O_{CP} is related to a linear combination of $C_{\rm nr}$ and $C_{\rm rn}$:

$$C_{\rm nr} - C_{\rm rn} = 9\langle O_{CP} \rangle. \tag{25}$$

Up to prefactors it can also be related to a spin observable at the level of the intermediate top-quarks:

$$\langle O_{CP} \rangle = -\frac{\kappa_\ell^2}{9} \langle (\mathbf{S}_t \times \mathbf{S}_{\bar{t}}) \cdot \hat{\mathbf{k}} \rangle . \tag{26}$$

One may consider also other CP-odd dileptonic triple correlations, for instance, a correlation where $\hat{\mathbf{k}}$ in Eq. (24) is replaced by the proton beam direction, i.e. sign$(y)\hat{\mathbf{p}}$. But this correlation has a very low sensitivity to resonant Higgs-boson induced CP violation, as an inspection of the corresponding squared S matrix element shows.

3.4. Difference between the leptonic azimuthal angles

Following Ref. [39] we construct a CP-sensitive angular observable ϕ^*_{CP} as follows. We identify the z-axis in the top and antitop rest frames with the direction of flight of the top quark in the $t\bar{t}$ ZMF, $\hat{\mathbf{k}}$. With respect to this z-axis we define the azimuthal angle ϕ^* between the charged leptons

$$\phi^* = \arccos(\hat{\boldsymbol{\ell}}_+^{\perp} \cdot \hat{\boldsymbol{\ell}}_-^{\perp}), \quad \phi^* \in [0, \pi]. \tag{27}$$

The unit 3-vector $\hat{\boldsymbol{\ell}}_+^{\perp}$ ($\hat{\boldsymbol{\ell}}_-^{\perp}$) defines the direction of the antilepton (lepton) perpendicular to $\hat{\mathbf{k}}$ in the top (antitop) rest frame ($\hat{\boldsymbol{\ell}}_\pm^{\perp} \cdot \hat{\mathbf{k}} = 0$):

$$\hat{\boldsymbol{\ell}}_\pm^{\perp} = \frac{\hat{\boldsymbol{\ell}}_\pm - (\hat{\boldsymbol{\ell}}_\pm \cdot \hat{\mathbf{k}})\hat{\mathbf{k}}}{\left|\hat{\boldsymbol{\ell}}_\pm - (\hat{\boldsymbol{\ell}}_\pm \cdot \hat{\mathbf{k}})\hat{\mathbf{k}}\right|}. \tag{28}$$

Similar to Ref. [39] we use the CP-odd triple product, $(\hat{\boldsymbol{\ell}}_+ \times \hat{\boldsymbol{\ell}}_-) \cdot \hat{\mathbf{k}}$, to construct a CP-sensitive observable from ϕ^* in order to probe the CP properties of the heavy Higgs bosons:

$$\phi^*_{CP} = \begin{cases} \phi^* & \text{if} \quad (\hat{\boldsymbol{\ell}}_+ \times \hat{\boldsymbol{\ell}}_-) \cdot \hat{\mathbf{k}} \geq 0 \\ 2\pi - \phi^* & \text{if} \quad (\hat{\boldsymbol{\ell}}_+ \times \hat{\boldsymbol{\ell}}_-) \cdot \hat{\mathbf{k}} < 0 \end{cases}, \quad \phi^*_{CP} \in [0, 2\pi]. \tag{29}$$

We are interested in the (normalized) distribution of this observable $\sigma^{-1} d\sigma / d\phi^*_{CP}$ because of its potential to discriminate between CP-even, CP-odd and CP-mixed heavy Higgs bosons. The parameters of scenarios 1a–1c (cf. Sec. 2) are chosen such that these cases can be directly compared and the sensitivity of ϕ^*_{CP} to the CP-properties of the heavy Higgs coupling to top quarks can be studied in detail.

4. Results

In this section we briefly describe the setup of our calculation. Furthermore, we present phenomenological results at NLO QCD for the distribution of the cross section with respect to the invariant mass of the top-quark pair and for the spin dependent observables introduced in the previous section.

4.1. Setup

For all observables introduced in the previous section we make predictions within the SM including QCD and weak corrections as well as predictions including the two additional (neutral) heavy Higgs bosons of the 2HDM parameter scenarios of Sec. 2. We stress that we take into account also the interference of the signal and background contributions at NLO. The contribution of the 125 GeV Higgs resonance is included in the SM predictions.

As far as the NLO QCD corrections are concerned we apply the same approximations to the non-SM contributions as we did in Ref. [10]. We use the heavy top mass limit including an effective K-factor rescaling to obtain the leading resonant contributions at NLO. For details we refer to Ref. [10].

The SM input parameters are chosen as in Ref. [10]. The top-quark mass renormalized in the on-shell scheme is set to

$$m_t = 173.34 \text{ GeV}. \tag{30}$$

For the values of the electromagnetic fine structure constant α and the gauge boson masses we use

$$\alpha = \frac{1}{129}, \quad m_W = 80.385 \text{ GeV}, \quad m_Z = 91.1876 \text{ GeV}. \tag{31}$$

For the parton distribution functions (PDFs) we employ the PDF set CT10nlo [40] which provides also the value of the strong coupling $\alpha_s(\mu_r)$ at the renormalization scale μ_r. As central scale we chose

$$\mu_r = \mu_f = \mu_0 \tag{32}$$

(μ_f denotes the factorization scale) with

$$\mu_0 = \frac{m_2 + m_3}{4}, \tag{33}$$

motivated by the choice $\mu_0 = m_H/2$ in the SM case (see, for instance, [41]). The uncertainties due to the residual dependence of the theoretical predictions on μ_f and μ_r are estimated by varying both scales simultaneously ($\mu_r = \mu_f \equiv \mu$) by a factor of two up and down. All results in this section are presented for proton-proton collisions at a center of mass energy of $\sqrt{s} = 13$ TeV and are thus applicable to the data collected during the LHC run II.

When calculating theoretical predictions for the observables defined in the previous section we always expand all ratios or normalized cross sections in the coupling constants. This is a consistent approximation when working in fixed order perturbation theory.

4.2. Top-quark pair invariant mass distribution

The invariant mass distribution of the $t\bar{t}$ pair, $d\sigma_{t\bar{t}}/dM_{t\bar{t}}$ where $M_{t\bar{t}} = \sqrt{(k_t + k_{\bar{t}})^2}$, is the basic observable in the search for heavy (Higgs) resonances in the $t\bar{t}$ channel. Here we compute this distribution at NLO in the SM and in the 2HDM using the parameter scenarios of Sec. 2. (These parameter sets are different from those used in Ref. [10].) In Sec. 4.3 we analyze top-spin dependent observables and compare the sensitivities of these observables and $d\sigma_{t\bar{t}}/dM_{t\bar{t}}$ to heavy Higgs boson effects.

The top-quark pair invariant mass distributions are displayed for scenarios 1a–1c and 2 in Figs. 1–4. For scenarios 1a–1c the peak-dip structure that results from the interference between signal and background is clearly visible for the lighter resonance at 400 GeV. For scenario 1b where the lighter resonance is a pseudoscalar we even observe a signal-to-background (S/B) ratio of about 18% in the $M_{t\bar{t}}$ bin from 380 GeV to 400 GeV. However, a bin width as small as 20 GeV cannot be attained by present experiments. For experimentally achievable bin widths of about 40 GeV (see for example Ref. [9]) in the lower $M_{t\bar{t}}$ range, the effect is 8%–13% depending on the bin position. In view of the recent ATLAS analysis [9] scenario 1b may be excluded. However, our main interest in this scenario is mostly to compare top spin effects induced by different heavy Higgs boson CP eigenstates and CP-mixed states and study the potential gain in sensitivity with respect to top-spin independent observables. The findings concerning the sensitivity of top-spin observables may also apply to other parameter scenarios. The resonance at 900 GeV in scenarios 1a–1c is barely visible in the $M_{t\bar{t}}$-distribution, mainly because of its large decay width.
In scenario 2 the heavy scalar and pseudoscalar resonances overlap and generate a single resonance structure between 700 GeV and 800 GeV. It is much more pronounced than the 900 GeV resonance in scenarios 1a–1c because of the smaller decay widths of the heavy Higgs bosons in scenario 2. The parameters of scenario 2 were chosen to allow a direct comparison with Ref. [42] where higher-order QCD corrections to the signal and interference have been estimated by applying a constant K-factor, K = 2. As our analysis shows, a simple K-factor rescaling as applied in Ref. [42] is questionable and is in general not sufficient to account for

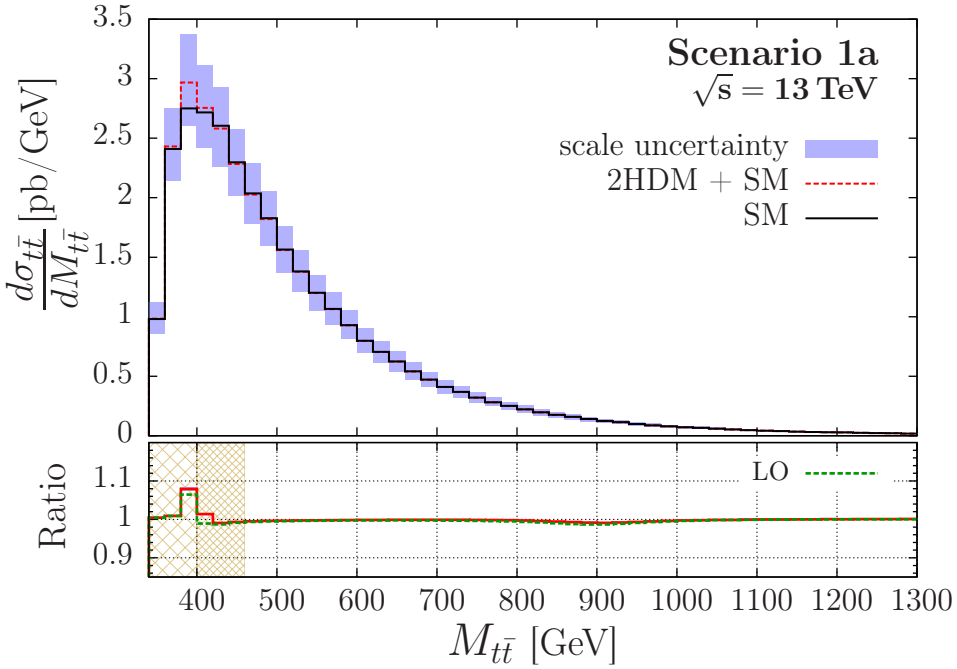

Figure 1: Distribution of the $t\bar{t}$ invariant mass, $M_{t\bar{t}}$, at NLO for scenario 1a. The upper pane shows the SM contribution (solid black) including NLO QCD and weak corrections and the sum of SM and 2HDM contributions (dashed red) at NLO QCD. The blue shaded area represents the scale uncertainty. The lower pane show the ratios of the $M_{t\bar{t}}$ distribution for the SM + 2HDM and SM at LO (dashed green) and NLO (solid red). The hatched regions in the ratio plots display the $M_{t\bar{t}}$ bins which are used to evaluate the spin dependent observables; cf. Sec. 4.3.

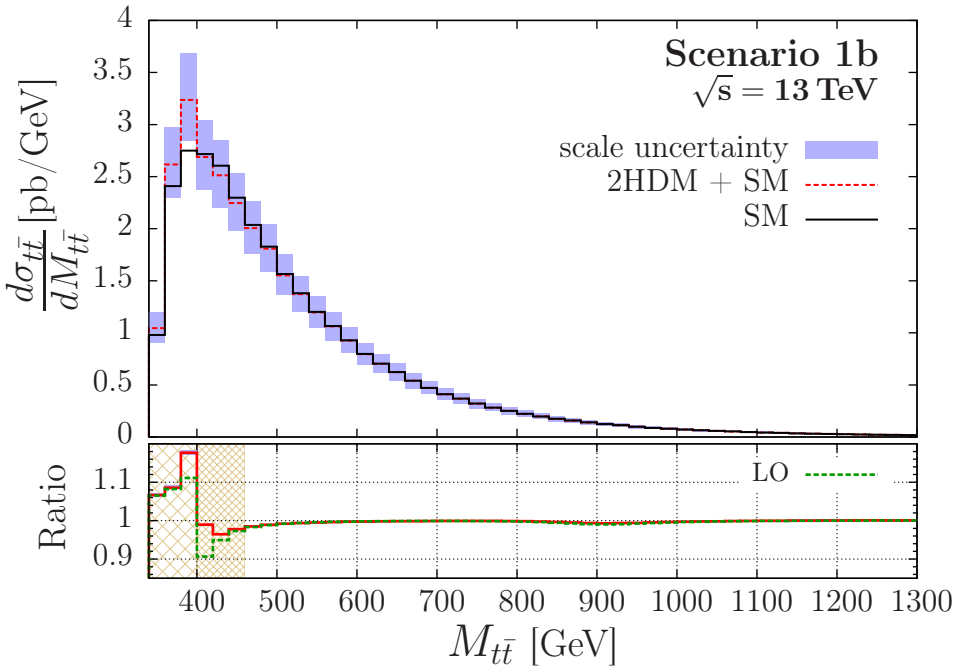

Figure 2: Same as Fig. 1 but for scenario 1b.

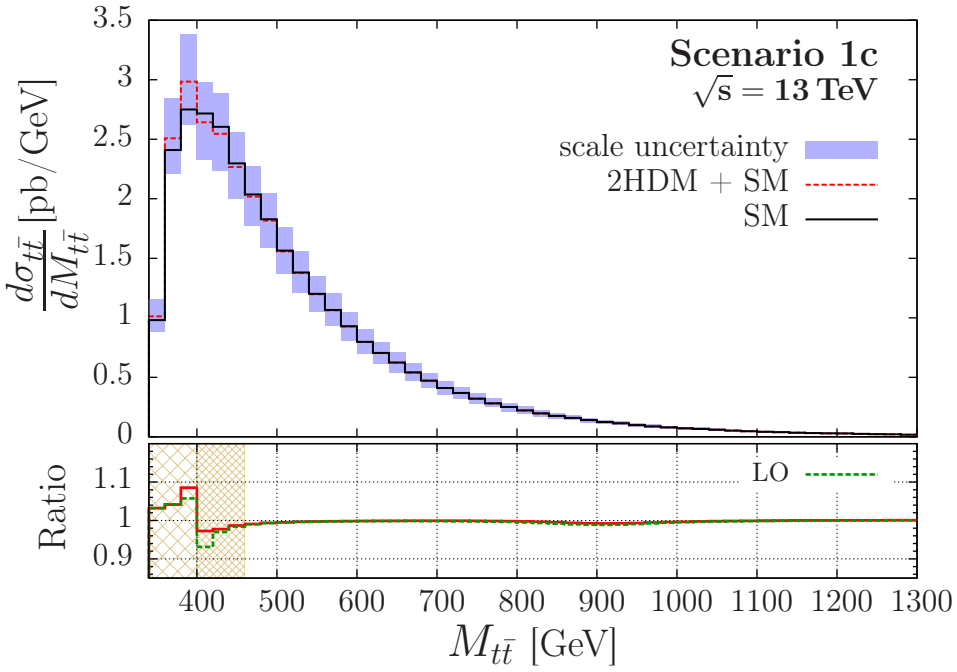

Figure 3: Same as Fig. 1 but for scenario 1c.

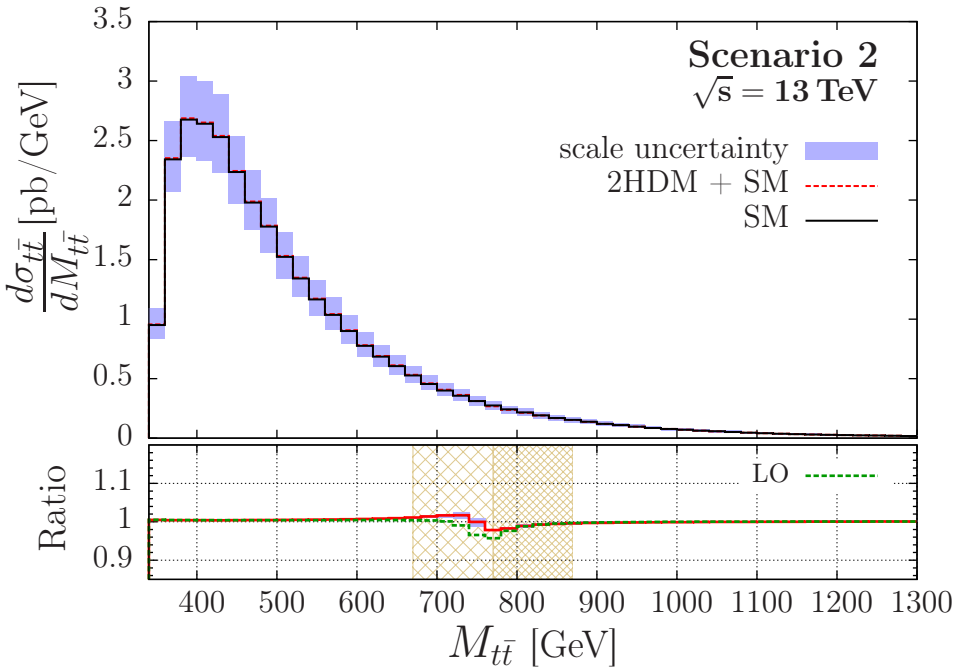

Figure 4: Same as Fig. 1 but for scenario 2.

higher order corrections to the $M_{t\bar{t}}$ distribution. In fact, within the approximations of the NLO corrections used here, the dip between 700 GeV and 800 GeV observed at LO (dashed-green line in Fig. 4) is reduced at NLO (solid-red line in Fig. 4). Hence, an experimental analysis using the naive K-factor rescaling would in this case lead to experimental bounds that are too strong—provided no effect will be seen.
We choose in the next section, as in Ref. [10], appropriate $M_{t\bar{t}}$ bins for evaluating the top-spin dependent observables, in order to avoid a cancellation due to the peak-dip structure in the $M_{t\bar{t}}$ spectrum. Thus we estimate, for the chosen parameter scenarios, with an optimized binning the maximal effects of heavy Higgs boson resonances in the $t\bar{t}$ decay channel. In Figs. 1–4 these $M_{t\bar{t}}$ bins are indicated by the hatched regions in the ratio plots. Since in an actual experimental analysis the optimal bin locations are unknown—unless a significant distortion in the $M_{t\bar{t}}$ distribution will be found—one would study the observables as functions of the bin location.

4.3. Spin dependent observables

We consider now the top-spin dependent observables introduced in Sec. 3 for the dileptonic $t\bar{t}$ events (10). As discussed in Sec. 4.2, we evaluate these observables within two $M_{t\bar{t}}$ bins in order to enhance the S/B ratio, namely $2m_t$–400 GeV and 400–460 GeV in scenarios 1a–1c and 670–770 GeV and 770-870 GeV in scenario 2. Results for the lepton angular correlations $C_{\rm hel}$, $C_{\rm nn}$, $C_{\rm rr}$ and D that correspond to P- and CP-even $t\bar{t}$ spin correlations are shown in

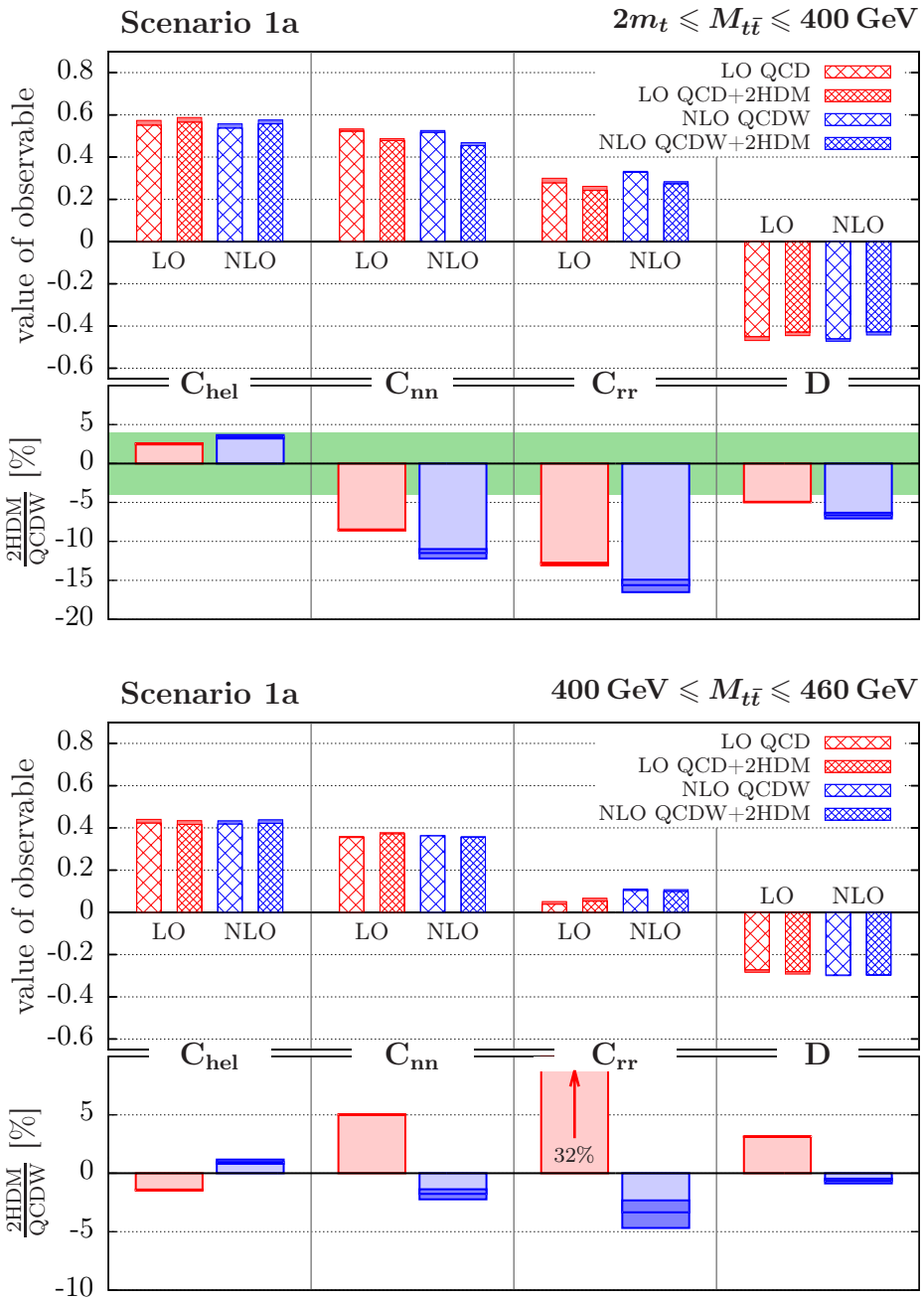

Figure 5: *P*- and *CP*-even spin correlations in scenario 1a for the LHC (13 TeV).

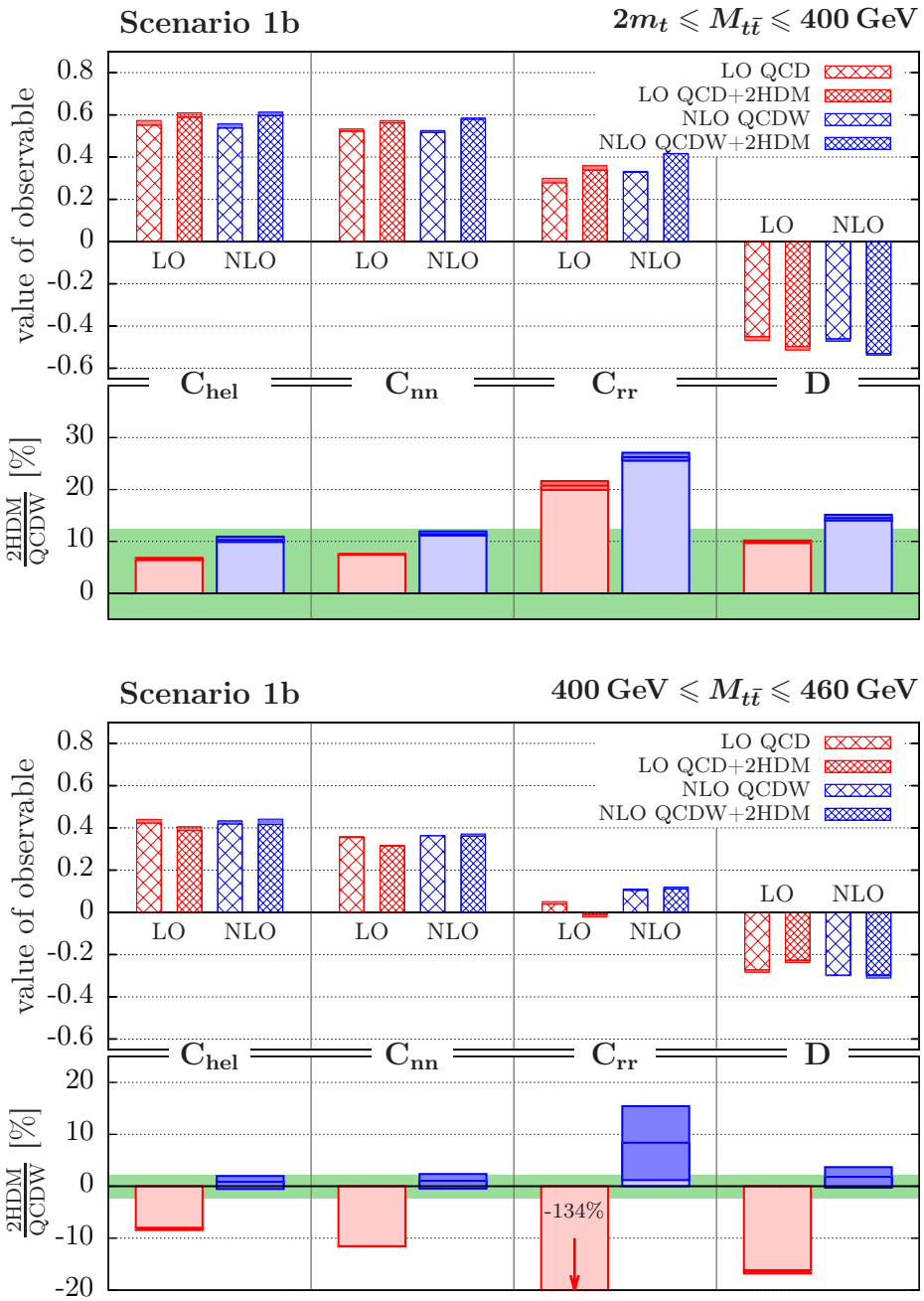

Figure 6: *P*- and *CP*-even spin correlations in scenario 1b for the LHC (13 TeV).

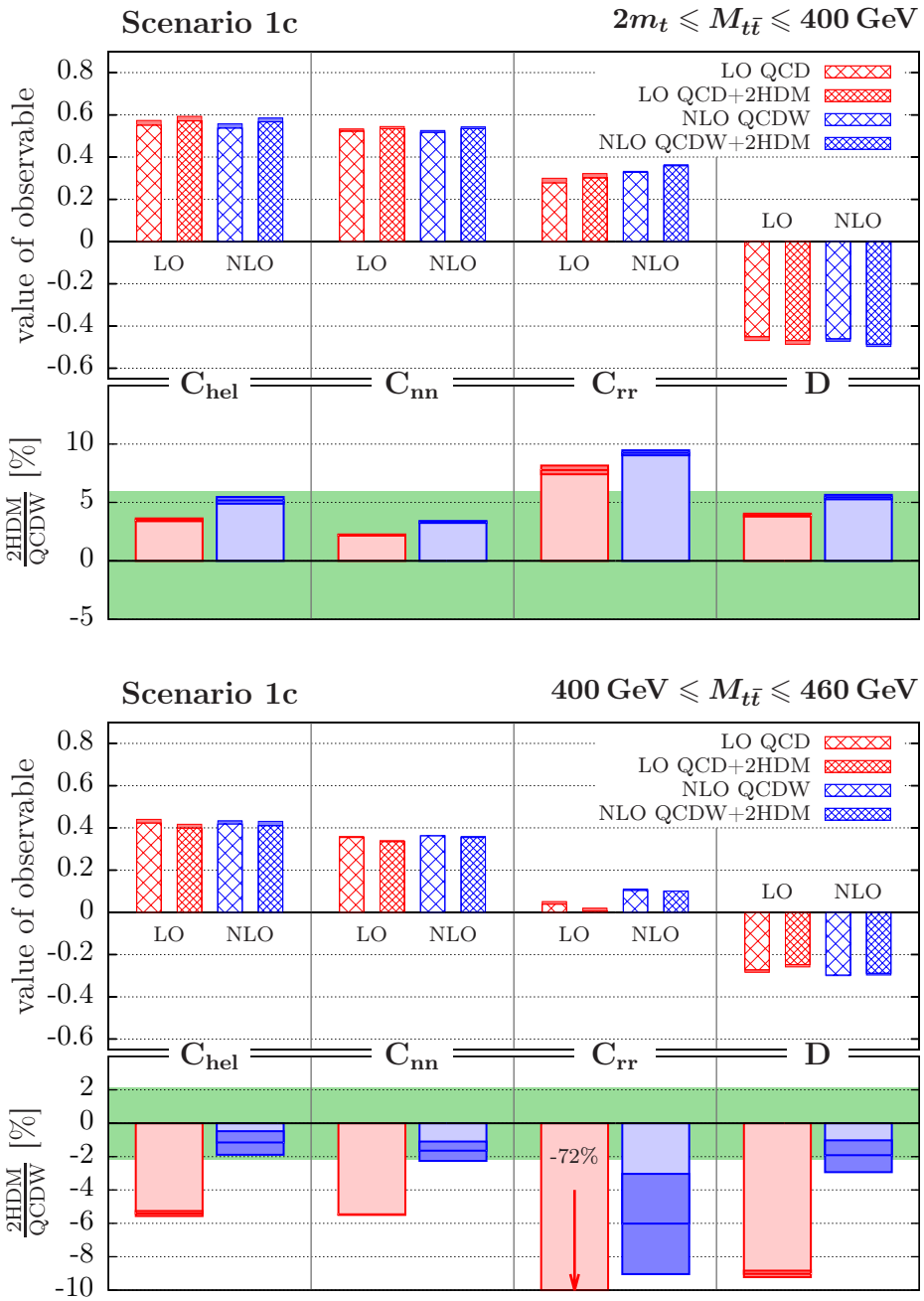

Figure 7: *P*- and *CP*-even spin correlations in scenario 1c for the LHC (13 TeV).

Figs. 5–7 for scenarios 1a–1c, respectively, and in Fig. 8 for scenario 2. In the upper panel of each plot the values of C_{hel}, C_{nn}, C_{rr} and D are displayed for the SM (coarse hatched) and for the SM + 2HDM contributions (fine hatched) including interference at LO (red) and NLO (blue). The solid filled regions of the bars represent the scale uncertainty estimated by varying the scale as described in Sec. 4.1.

In the lower panel of each plot the S/B ratio of the 2HDM contribution (including interference) and the SM prediction is shown at LO (red) and at NLO (blue). The darker parts of the bars represent the scale uncertainty of this ratio. In cases where the ratio takes on extreme values, the bars are only shown partially and the central value of the respective ratio is then given in the plot. The green shaded area in the ratio plots display, for comparison, the S/B ratio of the cross section within the respective $M_{t\bar{t}}$ bin at NLO. This ratio is obtained from the $M_{t\bar{t}}$ distributions computed in Sec. 4.2. We observe that for all parameter scenarios the S/B ratio of one or several of the four spin observables outreaches the green band. Thus these spin observables are, within the respective $M_{t\bar{t}}$ bin, more sensitive than the cross section. Notice that in some cases the S/B ratio of the cross section is very low and the green area is not (see for example the result for the high $M_{t\bar{t}}$ bin in Fig. 5) or only barely visible (Fig. 8).

For scenarios 1a–1c C_{rr} is the most sensitive of the four P- and CP-even spin correlation observables. The S/B ratio associated with C_{rr} is also larger in magnitude than that of the cross section—in case of scenario 1a almost by a factor of four in the lower $M_{t\bar{t}}$ bin. In the higher $M_{t\bar{t}}$ bin of 400–460 GeV the spin correlations and associated S/B ratios at NLO are smaller compared to those for the lower $M_{t\bar{t}}$ bin. In case of the observable C_{rr} the S/B ratios in the higher $M_{t\bar{t}}$ bin of 400–460 GeV at NLO deviate significantly from those at LO. The reason for this large difference is the fact that the $M_{t\bar{t}}$ distribution for this observable has a zero at LO within this $M_{t\bar{t}}$ bin—that this, it receives positive and negative contributions that (almost) cancel. This zero is shifted close to the bin boundary or even outside the bin when taking NLO corrections into account. Because the observable C_{rr} suffers from accidental (partial) cancellations at leading order it is very sensitive to NLO corrections. This does not signal a general breakdown of the perturbative expansion.

This circumstance should be seen as an artefact of the specific observable and is associated to a large extend with the chosen $M_{t\bar{t}}$ bin. Because of this (accidentally) large sensitivity to higher-order corrections, we observe large K-factors for C_{rr} in these specific cases: K = 1.7 for scenario 1a and |K| > 7 for scenarios 1b and 1c. Moreover, the NLO corrections lie outside of the LO uncertainty estimate. However, one may argue that the uncertainty estimate of the LO predictions are in any case unreliable because the spin observables studied here are defined as ratios where, for example, α_s cancels to leading order. (The situation becomes even worse at LO when ratios of ratios are considered.) Alternatively, one can compute a spin observable at NLO also without expanding the denominator and then compute the ratio R of the expanded and the unexpanded version. This ratio may be viewed as indicative of the convergence of the perturbative expansion. For the observable C_{rr} evaluated in the higher $M_{t\bar{t}}$ bin, we obtain $R = 1.2$, $R = 1.9$, and $R = 1.5$ for scenario 1a, 1b, and 1c, respectively, whereas for the other three spin observables we get $R \leq 1.1$. This shows again that in the $M_{t\bar{t}}$ bin of 400–460 GeV the observable C_{rr} is very sensitive to higher order corrections. It illustrates also the importance of

the NLO contributions to the spin observables. This example shows that one should be careful when using a specific spin observable in the search for heavy Higgs effects in $t\bar{t}$ data. Given a certain $M_{t\bar{t}}$ bin-choice, one should use in an agnostic experimental analysis spin observables that do not have a zero (in the above sense) at LO QCD.

As can be seen from Figs. 5–8 the uncertainty bands of the values of a spin observable at LO and NLO due to scale variations do not overlap in a number of cases. As stated before this is mainly because the spin correlations are ratios (see for example Eq. (12) and Eq. (20)) in which the μ_r dependence cancels at LO. The leading-order scale variation thus underestimates the effect of higher-order corrections and fails to give reliable uncertainty estimates.

The values of the four P- and CP-even spin correlations and the corresponding S/B ratios evaluated in the two $M_{t\bar{t}}$ bins displayed in Fig. 5 for scenario 1a are given in Tab. 9. In addition we list also the resulting values when no cuts on $M_{t\bar{t}}$ are imposed. Furthermore, the last column of this table contains the cross section for the dileptonic $t\bar{t}$ decay channel summed over $\ell, \ell' = e, \mu$, both for the low and high $M_{t\bar{t}}$ bin and inclusively, and the corresponding S/B ratios. The numbers substantiate what was already stated above: for the chosen bins and inclusively, one or several of the above spin observables are more sensitive to heavy Higgs-boson effects than the ratio of binned cross sections. In the low $M_{t\bar{t}}$ bin C_{nn}, C_{rr} and D feature S/B ratios larger than 6%, i.e., a significant sensitivity to the lighter of the two heavy Higgs bosons which is a scalar. Notice that not only C_{hel}, C_{nn}, and D but also C_{rr} has a reliable perturbative expansion in the lower $M_{t\bar{t}}$ bin.

The corresponding tables for the results presented in Fig. 6 and Fig. 7 are given in Appendix A (Tab. 12 and Tab. 13). The predictions for the low $M_{t\bar{t}}$ bin given in Tab. 12 for scenario 1b with a 400 GeV pseudoscalar show that all four spin correlations and the binned cross section have S/B$\gtrsim 10\%$. In the lower $M_{t\bar{t}}$ bin of scenario 1c only C_{rr} provides a S/B larger than that of the binned cross section, namely $\sim 9\%$ (cf. Tab. 13). Both for scenarios 1b and 1c the perturbative expansions of the spin correlations in the low $M_{t\bar{t}}$ bin, in particular of C_{rr}, are reliable.

Scenarios 1a–1c feature strong Higgs-boson signals and experimental analyses of the $M_{t\bar{t}}$ distribution might already be sensitive to these effects. In scenario 2 the signal is much weaker which makes it difficult to constrain this scenario with the $M_{t\bar{t}}$ distribution. As can be seen from Fig. 8—and from the corresponding numbers in Tab. 14 of Appendix A—the S/B ratio of the cross section (green band) is very small in both $M_{t\bar{t}}$ bins, S/B $\lesssim 1\%$. As in scenarios 1a–1c we encounter here also the problem of zero(s) of spin observables. In this case the observables C_{hel} and D have zeros in the $M_{t\bar{t}}$ bin 670–770 GeV at LO which are shifted to the other $M_{t\bar{t}}$ bin 770–870 GeV at NLO. This leads to a high sensitivity of C_{hel} and D to NLO corrections which affects the robustness of the prediction. The observables C_{nn} and C_{rr} have a reliable perturbative expansion in these $M_{t\bar{t}}$ bins. However, taking the scale uncertainty into account their sensitivity is not sufficient to constrain this model. One way to remedy this is to evaluate C_{hel}, which is the most sensitive of the four spin correlations in this scenario, within 500 GeV $\leq M_{t\bar{t}} \leq$ 750 GeV. This yields a S/B ratio of 4% as compared to the cross section S/B ratio of 0.7% at NLO, and the prediction is also more robust with respect to NLO corrections (K = 1.3, R = 1.1). The reason for having chosen the above bins is that our prediction of

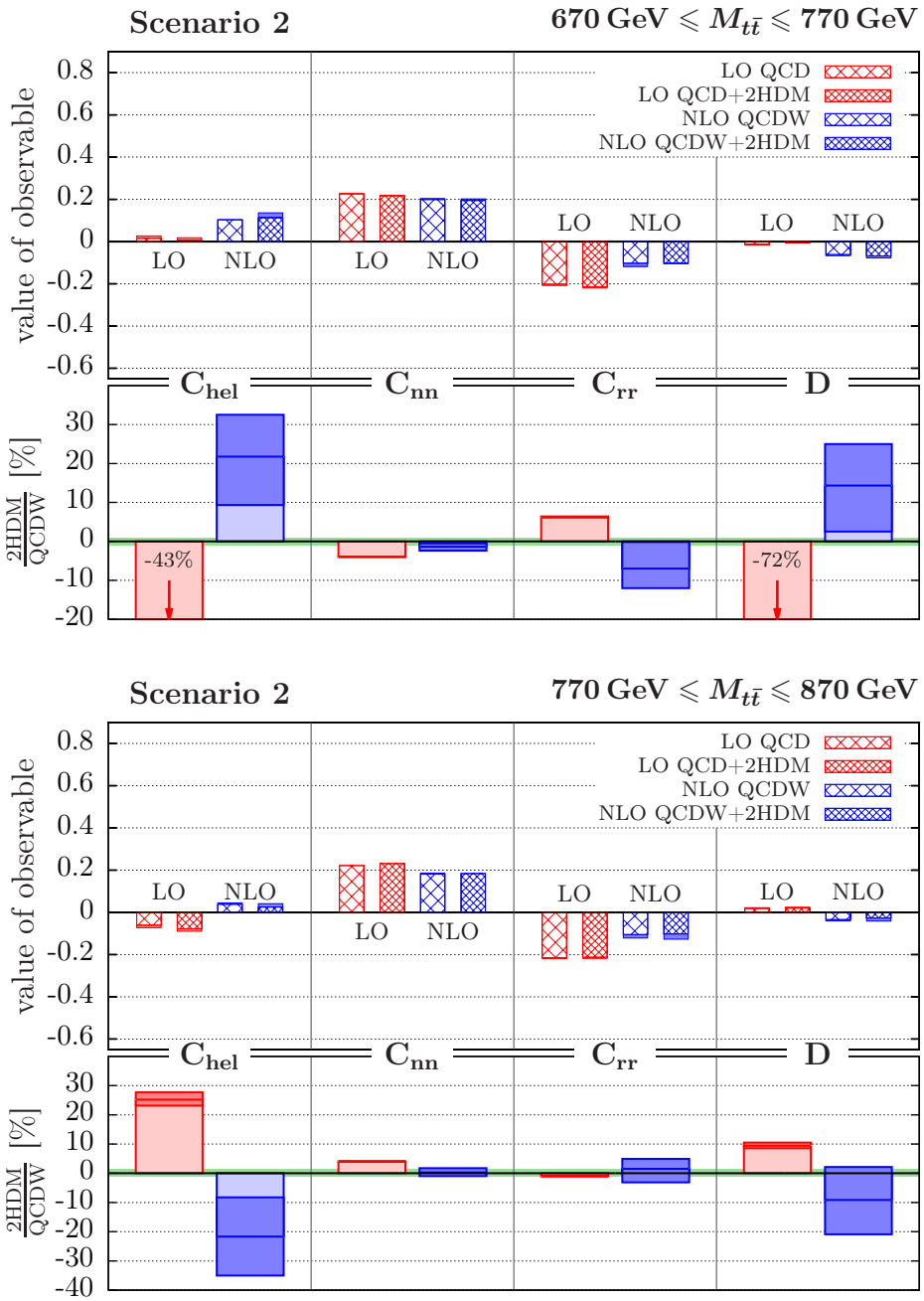

Figure 8: *P*- and *CP*-even spin correlations in scenario 2 for the LHC (13 TeV).

the heavy Higgs effects at NLO is most accurate within the Higgs resonance region. Choosing instead an $M_{t\bar{t}}$ range of 500–750 GeV will affect the accuracy of our approach. Thus, a more careful investigation of the uncertainties of $C_{\rm hel}$ due to these approximations would be necessary but is left for future work.

The spin correlations $C_{\rm hel}$, $C_{\rm rr}$, and $C_{\rm nn}$ were recently computed, inclusively in $M_{t\bar{t}}$, at NLO QCD including weak interaction corrections also in [13], and our corresponding predictions in Tabs. 9, 12, 13 and 14 agree with these results[3]. The spin correlations $C_{\rm hel}$ and $C_{\rm rr}$, $C_{\rm nn}$ were recently measured in dileptonic $t\bar{t}$ events, inclusively in $M_{t\bar{t}}$, at the LHC(8 TeV) in [31, 32] and [32], respectively. The results, corrected to parton level in the full phase space, agree with respective SM predictions. At 8 TeV center-of-mass energy the contributions of the heavy Higgs resonances of our parameter scenarios to these observables are smaller in magnitude than at 13 TeV, and we have checked that these contributions are in accord with the results of [31, 32] within the experimental uncertainties.

The observables $C_{\rm hel}$, $C_{\rm nn}$, $C_{\rm rr}$, and D no not provide any information about the CP nature of the Higgs resonances. The P- and CP-odd triple correlation O_{CP} given in Eq. (24) allows to search for (non-standard) CP violation in dileptonic $t\bar{t}$ events, in particular for effects induced by heavy Higgs resonances that are CP mixtures. Among the four scenarios studied in this paper only the CP-violating scenario 1c leads to a non-vanishing $\langle O_{CP}\rangle$. The results for the expectation value $\langle O_{CP}\rangle$ for dileptonic $t\bar{t}$ events at 13 TeV in the low and high $M_{t\bar{t}}$ bin and inclusively in $M_{t\bar{t}}$ are presented in Tab. 10.

The expectation value $\langle O_{CP}\rangle$ is below the percent level even in the bins around 400 GeV where the CP-violating effect is caused by the resonant production of the 400 GeV Higgs resonance of indefinite parity. The inclusive expectation value is an order of magnitude smaller which is due to partial cancellations of the two heavy Higgs boson contributions. We note that $\langle O_{CP}\rangle$ can also be obtained from the measurement of the difference of two off-diagonal correlations cf. Eq. (25). This difference of spin correlations was recently measured by ATLAS for dileptonic $t\bar{t}$ events at 8 TeV. At the parton level in the full phase-space the result $C_{nr} - C_{rn} = -0.006 \pm 0.108$ was obtained [32]. We checked that the value of $9\langle O_{CP}\rangle$ at 8 TeV in scenario 1c is in accord with this result within the experimental uncertainty.

Table 11 contains our predictions, for scenarios 1a - 1c, of the coefficient $B_t(k)$ that measures the longitudinal polarization of the top quark in the helicity basis (cf. Eq. (20)). The predictions apply to dileptonic and to $\ell^+ +$ jets events. A non-zero value of B_t, which requires P-violating interactions, is generated in the SM by the weak interactions. In scenarios 1a and 1b the neutral Higgs interactions are P-conserving. Thus in these scenarios B_t is zero at LO and given at NLO by the results listed in column 'QCDW' of Tab. 11—neglecting contributions from the charged Higgs boson. They are very small because we assume $H^\pm$ to be very heavy. In scenario 1c the neutral Higgs bosons induce P-violating effects already at LO and the resulting values of B_t at NLO within the SM + 2HDM differ from those of the SM. Although the S/B ratio can be significantly enhanced by $M_{t\bar{t}}$ cuts the effects remain below the

[3]The results presented here and those given in Ref. [13] are not completely identical, because in Ref. [13] the scale choice $m_t/2 \le \mu \le 2m_t$ was used.

Table 9: *P*- and *CP*-even spin correlations and dileptonic cross section in scenario 1a for the LHC(13 TeV).

			C_{hel}	C_{nn}	C_{rr}	D	$\sigma_{t\bar{t}}\times$BR [pb]
$2m_t \leq M_{t\bar{t}} \leq 400$ GeV	LO	2HDM+QCD	$0.576^{+0.011}_{-0.011}$	$0.483^{+0.005}_{-0.005}$	$0.252^{+0.010}_{-0.010}$	$-0.437^{+0.009}_{-0.009}$	$3.70^{+0.89}_{-0.68}$
		QCD	$0.562^{+0.011}_{-0.011}$	$0.528^{+0.005}_{-0.005}$	$0.289^{+0.011}_{-0.011}$	$-0.459^{+0.009}_{-0.009}$	$3.58^{+0.85}_{-0.65}$
		$\frac{\text{2HDM}}{\text{QCD}}$ [%]	$2.52^{+0.08}_{-0.08}$	$-8.52^{+0.06}_{-0.07}$	$-12.9^{+0.2}_{-0.2}$	$-4.93^{+0.03}_{-0.04}$	$3.35^{+0.05}_{-0.05}$
	NLO	2HDM+QCDW	$0.567^{+0.008}_{-0.010}$	$0.462^{+0.006}_{-0.008}$	$0.278^{+0.005}_{-0.005}$	$-0.435^{+0.007}_{-0.007}$	$6.30^{+0.86}_{-0.76}$
		QCDW	$0.548^{+0.009}_{-0.011}$	$0.522^{+0.004}_{-0.005}$	$0.330^{+0.003}_{-0.002}$	$-0.466^{+0.006}_{-0.005}$	$6.06^{+0.81}_{-0.73}$
		$\frac{\text{2HDM}}{\text{QCDW}}$ [%]	$3.38^{+0.28}_{-0.17}$	$-11.5^{+0.5}_{-0.7}$	$-15.6^{+0.7}_{-0.9}$	$-6.64^{+0.33}_{-0.41}$	$3.97^{+0.24}_{-0.18}$
$400 \leq M_{t\bar{t}} \leq 460$ GeV	LO	2HDM+QCD	$0.426^{+0.009}_{-0.009}$	$0.374^{+0.002}_{-0.002}$	$0.060^{+0.006}_{-0.006}$	$-0.286^{+0.006}_{-0.006}$	$4.49^{+1.10}_{-0.86}$
		QCD	$0.432^{+0.009}_{-0.009}$	$0.356^{+0.002}_{-0.002}$	$0.045^{+0.006}_{-0.006}$	$-0.278^{+0.006}_{-0.006}$	$4.54^{+1.10}_{-0.87}$
		$\frac{\text{2HDM}}{\text{QCD}}$ [%]	$-1.43^{+0.04}_{-0.04}$	$5.01^{+0.03}_{-0.03}$	$32.1^{+5.0}_{-3.0}$	$3.14^{+0.01}_{-0.01}$	$-1.08^{+0.01}_{-0.01}$
	NLO	2HDM+QCDW	$0.430^{+0.008}_{-0.008}$	$0.356^{+0.001}_{-0.001}$	$0.103^{+0.005}_{-0.004}$	$-0.296^{+0.001}_{-0.001}$	$7.52^{+0.98}_{-0.91}$
		QCDW	$0.426^{+0.007}_{-0.007}$	$0.362^{+0.001}_{-0.000}$	$0.107^{+0.004}_{-0.003}$	$-0.298^{+0.001}_{-0.001}$	$7.53^{+0.98}_{-0.91}$
		$\frac{\text{2HDM}}{\text{QCDW}}$ [%]	$0.959^{+0.219}_{-0.150}$	$-1.76^{+0.39}_{-0.47}$	$-3.34^{+1.00}_{-1.30}$	$-0.651^{+0.194}_{-0.222}$	$-0.017^{+0.031}_{-0.012}$
incl. in $M_{t\bar{t}}$	LO	2HDM+QCD	$0.298^{+0.003}_{-0.004}$	$0.328^{+0.000}_{-0.000}$	$-0.017^{+0.002}_{-0.003}$	$-0.203^{+0.002}_{-0.002}$	$18.7^{+5.0}_{-4.0}$
		QCD	$0.297^{+0.003}_{-0.004}$	$0.329^{+0.000}_{-0.001}$	$-0.017^{+0.002}_{-0.003}$	$-0.203^{+0.002}_{-0.002}$	$18.6^{+5.0}_{-4.0}$
		$\frac{\text{2HDM}}{\text{QCD}}$ [%]	$0.313^{+0.029}_{-0.031}$	$-0.277^{+0.022}_{-0.019}$	$2.67^{+0.19}_{-0.21}$	$-0.071^{+0.005}_{-0.004}$	$0.133^{+0.009}_{-0.011}$
	NLO	2HDM+QCDW	$0.339^{+0.004}_{-0.002}$	$0.317^{+0.002}_{-0.002}$	$0.059^{+0.006}_{-0.004}$	$-0.238^{+0.000}_{-0.001}$	$30.5^{+4.0}_{-4.0}$
		QCDW	$0.333^{+0.003}_{-0.002}$	$0.327^{+0.001}_{-0.001}$	$0.065^{+0.006}_{-0.004}$	$-0.242^{+0.000}_{-0.001}$	$30.3^{+4.0}_{-4.0}$
		$\frac{\text{2HDM}}{\text{QCDW}}$ [%]	$1.99^{+0.03}_{-0.03}$	$-2.95^{+0.10}_{-0.13}$	$-9.98^{+0.17}_{-0.09}$	$-1.31^{+0.11}_{-0.14}$	$0.631^{+0.044}_{-0.027}$

Table 10: The expectation value $\langle O_{CP} \rangle$ in scenario 1c for dileptonic $t\bar{t}$ events at the LHC at 13 TeV.

$M_{t\bar{t}}$ [GeV]	LO 2HDM	NLO 2HDM
$[2m_t,400]$	$-0.549^{+0.007}_{-0.007}\times10^{-2}$	$-0.824^{+0.024}_{-0.029}\times10^{-2}$
$[400,460]$	$0.587^{+0.005}_{-0.005}\times10^{-2}$	$0.127^{+0.062}_{-0.054}\times10^{-2}$
incl.	$0.666^{+0.005}_{-0.005}\times10^{-3}$	$-0.814^{+0.008}_{-0.020}\times10^{-3}$

Table 11: The coefficient $B_t(k)$, which measures the longitudinal polarization of the top quark in the helicity basis in the SM and in scenario 1c, for dileptonic and semileptonic $t\bar{t}$ events at the LHC(13 TeV). In scenarios 1a and 1b B_t receives no contributions from neutral Higgs bosons. In these scenarios B_t is given by the QCDW value in the table.

$M_{t\bar{t}}$ [GeV]	LO	NLO		
	2HDM	2HDM+QCDW	QCDW	$\frac{\text{2HDM}}{\text{QCDW}}$
$[2m_t,400]$	$0.110^{+0.001}_{-0.001}\times10^{-1}$	$0.492^{+0.020}_{+0.014}\times10^{-2}$	$0.169^{+0.120}_{-0.098}\times10^{-2}$	$1.91^{+4.30}_{-1.20}$
$[400,460]$	$-0.769^{+0.007}_{-0.007}\times10^{-2}$	$0.403^{+0.313}_{-0.293}\times10^{-2}$	$0.316^{+0.174}_{-0.139}\times10^{-2}$	$0.275^{+0.187}_{-0.655}$
incl.	$-0.600^{+0.024}_{-0.026}\times10^{-3}$	$0.617^{+0.227}_{-0.185}\times10^{-2}$	$0.553^{+0.209}_{-0.164}\times10^{-2}$	$0.114^{-0.006}_{-0.007}$

percent level and exhibit large scale uncertainties. In scenario 2 the neutral Higgs interactions are P-conserving. Thus, the NLO predictions given in column 'QCDW' of Tab. 11 apply also to this scenario, provided the same scale choices are made as in scenarios 1a–1c. Our inclusive QCDW prediction of B_t given in Tab. 11 agrees with the corresponding prediction of [13]. (Notice that our scale choices differ from those of [13].) The polarization observable B_t was measured inclusively in $M_{t\bar{t}}$ at 8 TeV by the ATLAS and CMS experiment [32, 43], with an absolute experimental uncertainty of a few percent. We checked that our inclusive SM+2HDM predictions at 8 TeV are in accord with these measurements.

Finally we analyze the normalized leptonic azimuthal-angle difference ϕ^*_{CP} defined in Sec. 3.4. Observables of this type have the potential to yield information about the CP properties of the Higgs bosons [17, 18, 39]. We compute the distribution of ϕ^*_{CP} for scenarios 1a - 1c at NLO in the SM and in the SM + 2HDM in the low and high $M_{t\bar{t}}$ bins that were already chosen above for evaluating the other spin observables. These scenarios were chosen on purpose such that they

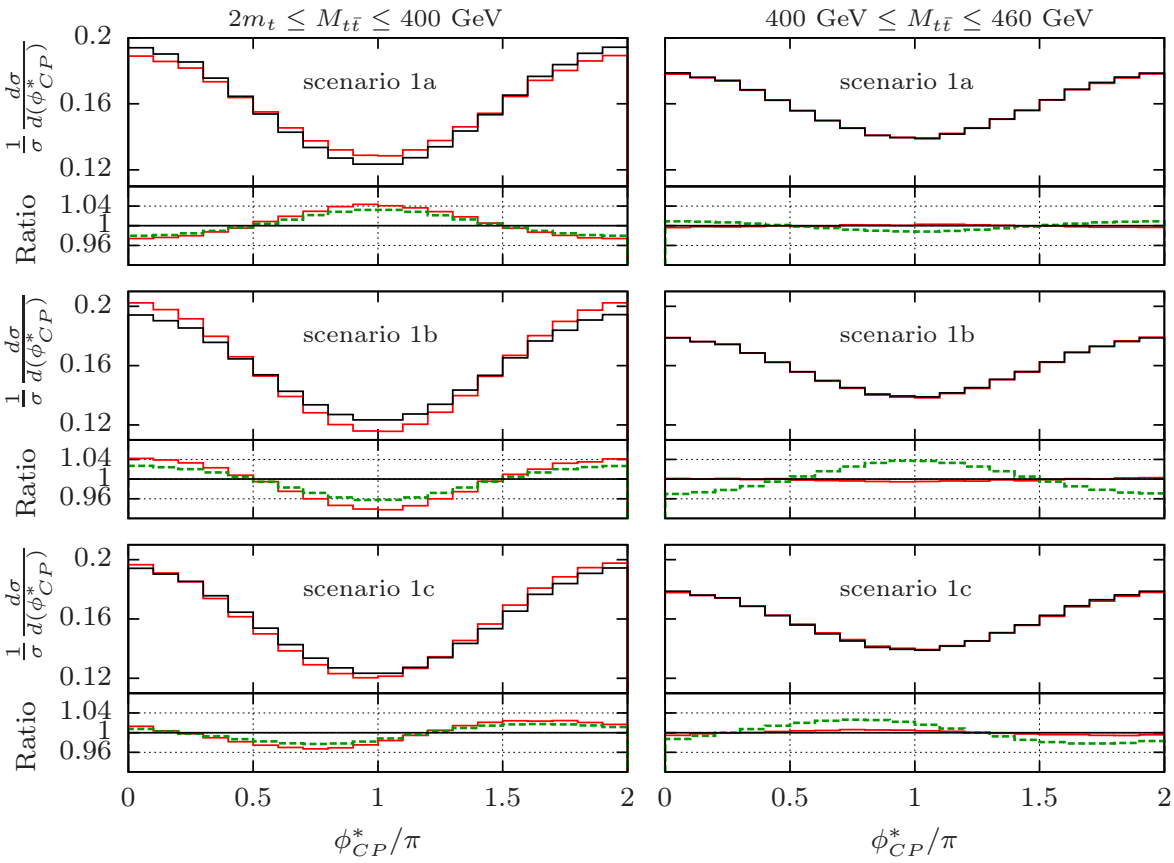

Figure 9: Upper panels: The normalized distribution of ϕ^*_{CP} for scenarios 1a–1c in two different $M_{t\bar{t}}$ bins. The NLO prediction in the SM and in the SM + 2HDM is displayed in black and in red, respectively. Lower panels: The curves in red (green) are the ratios (SM+2HDM)/SM at NLO (LO).

contain a scalar (1a), a pseudoscalar (1b), or a CP-mixed (1c) Higgs boson of the same mass (400 GeV). Our aim is to investigate the discriminating power of ϕ^*_{CP} with respect to the CP nature of this boson at NLO. (An observable similar to ϕ^*_{CP} with a different phase convention was analyzed at LO in Ref. [18], including the interference with the QCD background.)

Our results for the normalized distribution of ϕ^*_{CP} in scenarios 1a–1c are displayed in the upper panels of Fig. 9, on the left (right) for the low (high) $M_{t\bar{t}}$ bin. The distributions in black and red are the predictions within the SM and the SM + 2HDM, respectively, at NLO. The effect of scale variations is very small and not visible in these plots. In the lower panels the ratios R=(SM+2HDM)/SM are plotted. Here the green-dashed and red-solid lines refer to the LO and NLO predictions, respectively. These ratios have a trigonometric function-like shape. The ratios R in the low $M_{t\bar{t}}$ bin have some sensitivity to the CP nature of the 400 GeV Higgs boson. While the maximum (minimum) of R is located at $\phi^*_{CP} = \pi$ ($\phi^*_{CP} = 0, 2\pi$) if the 400 GeV Higgs boson is a scalar, it is shifted to $\phi^*_{CP} = 0, 2\pi$ ($\phi^*_{CP} = \pi$) if this boson is a pseudoscalar. If the 400 GeV Higgs boson is a CP mixture as in scenario 1c the maximum and minimum of R are located at $\phi^*_{CP} \neq 0, \pi, 2\pi$. The locations depend on the relative strengths and phases of the scalar and pseudoscalar Yukawa couplings of the 400 GeV Higgs boson to top quarks. In contrast to the tau-pair decay channel of a Higgs boson studied in Ref. [39], the background is not flat in ϕ^*_{CP} and the signal-background interference is not negligible in the case at hand. The large non-resonant SM background contribution leads to a rather small signal-to-background ratio of S/B $\lesssim 6\%$. We recall that in these scenarios the 400 GeV Higgs signal is significant in the $M_{t\bar{t}}$ distribution and in spin observables studied above. We therefore expect even lower S/B ratios for weaker Higgs signals, which poses an even bigger challenge to determine the Higgs CP properties with this observable. The NLO corrections enhance the S/B ratio only slightly.

5. Summary and conclusions

We considered, in continuation of our previous work [10], the production of top-quark pairs at the LHC (13 TeV) and their subsequent decay to dileptonic final states and analyzed, within the type-II 2HDM extension of the SM, the sensitivity of top-spin dependent observables to the resonant production of heavy Higgs bosons. NLO QCD corrections to the Higgs-boson signal in the $t\bar{t}$ channel and NLO QCD and weak interaction corrections to the non-resonant $t\bar{t}$ background were taken into account, including the signal-background interference at NLO. We determined, for four different 2HDM parameter scenarios, a number of leptonic angular correlations and distributions that correspond to $t\bar{t}$ spin correlations and to the longitudinal top-quark polarization. We computed also the $t\bar{t}$ invariant mass distribution, which is the basic observable in the search for heavy Higgs bosons in $t\bar{t}$ events, in order to assess the gain in sensitivity if such a search is accompanied by top-spin dependent observables. Our analysis shows that $t\bar{t}$ spin correlations have the potential to substantially increase the sensitivity of the $t\bar{t}$ channel to heavy Higgs resonances if they are evaluated in judiciously chosen $M_{t\bar{t}}$ bins. NLO corrections are, needless to say, important for assessing whether a specific observable has a

robust perturbative expansion within a chosen $M_{t\bar{t}}$ bin and for estimating the uncertainties due to scale variations.

The observable B_t that corresponds to the longitudinal top-quark polarization and the triple product correlation O_{CP} analyzed above are sensitive to P-violating, respectively P- and CP-violating interactions. We studied the effects of heavy Higgs resonances of undefined CP parity on these observables for a CP-violating 2HDM scenario. We found that the effects are small, even if these observables are evaluated in appropriate $M_{t\bar{t}}$ bins. Our studies indicate that measurement of these (dimensionless) observables with a precision of $\sim 10^{-3}$ would be required in order to reach meaningful sensitivities to P- and CP-violating heavy Higgs-boson effects.

Furthermore, we studied the potential of the lepton azimuthal angle distribution $d\sigma/d\phi^*_{CP}$ for pinning down the CP properties of a heavy Higgs resonance in the dileptonic $t\bar{t}$ events. This observable allows to construct a ratio whose shape shows significant differences with respect to effects of Higgs bosons of different CP nature. Yet the signal-to-background ratio is only about S/B $\lesssim 6\%$ because of the large SM background and the non-negligible signal-background interference.

Our detailed studies show that including top-spin dependent observables in the toolkit for the search for heavy Higgs-boson resonances in the $t\bar{t}$ channel can significantly enhance the sensitivity of these explorations. Although the results of this paper were obtained for specific parameter settings within the 2HDM, we believe that this conclusion remains valid also for other SM extensions that predict heavy neutral Higgs bosons with unsuppressed couplings to top quarks. We showed also that inclusion of NLO QCD corrections is important in this type of analysis. In particular, we illustrated with a concrete example that a naive K-factor approach is in general not sufficient for obtaining reliable predictions.

Acknowledgments

We thank C. Mellein for collaboration at an early stage of this project. P. Galler was supported by Deutsche Forschungsgemeinschaft through Graduiertenkolleg Grant No. GRK 1504. The work of Z.-G. Si was supported by National Natural Science Foundation of China and by Natural Science Foundation of Shandong Province.

A. Results for the P- and CP-even spin correlations and cross section in scenarios 1b, 1c, and 2

We present the results displayed in Figs. 6, 7, and 8 for the parameter scenarios 1b, 1c, and 2, respectively, in the tables of this appendix. They contain the values of the four P- and CP-even spin correlations and the corresponding S/B ratios evaluated in two $M_{t\bar{t}}$ bins and, in addition, in the whole $M_{t\bar{t}}$ range. Moreover, the cross section for the dileptonic $t\bar{t}$ decay

channel summed over $\ell, \ell' = e, \mu$ is given in the last column of this table, both for the low and high $M_{t\bar{t}}$ bin and inclusively, and the corresponding S/B ratios. These results are discussed in Sec. 4.3.

Table 12: P- and CP-even spin correlations and dileptonic cross section in scenario 1b for the LHC(13 TeV).

			C_{hel}	C_{nn}	C_{rr}	D	$\sigma_{t\bar{t}}\times$BR [pb]
$2m_t \leq M_{t\bar{t}} \leq 400$ GeV	LO	2HDM+QCD	$0.599^{+0.011}_{-0.011}$	$0.567^{+0.005}_{-0.005}$	$0.349^{+0.011}_{-0.010}$	$-0.505^{+0.009}_{-0.009}$	$3.91^{+0.94}_{-0.72}$
		QCD	$0.562^{+0.011}_{-0.011}$	$0.528^{+0.005}_{-0.005}$	$0.289^{+0.011}_{-0.011}$	$-0.459^{+0.009}_{-0.009}$	$3.58^{+0.85}_{-0.65}$
		$\frac{\text{2HDM}}{\text{QCD}}$ [%]	$6.61^{+0.23}_{-0.22}$	$7.51^{+0.08}_{-0.08}$	$20.7^{+0.9}_{-0.8}$	$9.92^{+0.26}_{-0.25}$	$9.28^{+0.12}_{-0.11}$
	NLO	2HDM+QCDW	$0.605^{+0.008}_{-0.009}$	$0.582^{+0.003}_{-0.003}$	$0.416^{+0.001}_{+0.000}$	$-0.534^{+0.004}_{-0.004}$	$6.81^{+0.95}_{-0.84}$
		QCDW	$0.548^{+0.009}_{-0.011}$	$0.522^{+0.004}_{-0.005}$	$0.330^{+0.003}_{-0.002}$	$-0.466^{+0.006}_{-0.005}$	$6.06^{+0.81}_{-0.73}$
		$\frac{\text{2HDM}}{\text{QCDW}}$ [%]	$10.3^{+0.6}_{-0.4}$	$11.4^{+0.5}_{-0.3}$	$26.2^{+0.9}_{-0.7}$	$14.5^{+0.7}_{-0.5}$	$12.3^{+0.5}_{-0.5}$
$400 \leq M_{t\bar{t}} \leq 460$ GeV	LO	2HDM+QCD	$0.396^{+0.009}_{-0.009}$	$0.315^{+0.002}_{-0.002}$	$-0.016^{+0.006}_{-0.006}$	$-0.232^{+0.006}_{-0.006}$	$4.28^{+1.10}_{-0.81}$
		QCD	$0.432^{+0.009}_{-0.009}$	$0.356^{+0.002}_{-0.002}$	$0.045^{+0.006}_{-0.006}$	$-0.278^{+0.006}_{-0.006}$	$4.54^{+1.10}_{-0.87}$
		$\frac{\text{2HDM}}{\text{QCD}}$ [%]	$-8.20^{+0.22}_{-0.23}$	$-11.6^{0.0}_{-0.0}$	-134^{+16}_{-21}	$-16.5^{+0.3}_{-0.3}$	$-5.87^{+0.05}_{-0.05}$
	NLO	2HDM+QCDW	$0.429^{+0.012}_{-0.013}$	$0.366^{+0.005}_{-0.005}$	$0.116^{+0.004}_{-0.004}$	$-0.304^{+0.008}_{-0.007}$	$7.36^{+0.96}_{-0.88}$
		QCDW	$0.426^{+0.007}_{-0.007}$	$0.362^{+0.001}_{-0.000}$	$0.107^{+0.004}_{-0.003}$	$-0.298^{+0.001}_{-0.001}$	$7.53^{+0.98}_{-0.91}$
		$\frac{\text{2HDM}}{\text{QCDW}}$ [%]	$0.844^{+1.150}_{-1.370}$	$1.06^{+1.30}_{-1.50}$	$8.39^{+7.00}_{-7.20}$	$1.83^{+1.90}_{-2.10}$	$-2.25^{+0.09}_{-0.04}$
incl. in $M_{t\bar{t}}$	LO	2HDM+QCD	$0.297^{+0.003}_{-0.004}$	$0.329^{+0.000}_{-0.001}$	$-0.017^{+0.002}_{-0.002}$	$-0.203^{+0.002}_{-0.002}$	$18.7^{+5.0}_{-4.0}$
		QCD	$0.297^{+0.003}_{-0.004}$	$0.329^{+0.000}_{-0.001}$	$-0.017^{+0.002}_{-0.003}$	$-0.203^{+0.002}_{-0.002}$	$18.6^{+5.0}_{-4.0}$
		$\frac{\text{2HDM}}{\text{QCD}}$ [%]	$0.043^{+0.042}_{-0.045}$	$-0.032^{+0.026}_{-0.029}$	$0.261^{+1.140}_{-0.781}$	$-0.004^{+0.059}_{-0.064}$	$0.018^{+0.017}_{-0.019}$
	NLO	2HDM+QCDW	$0.351^{+0.004}_{-0.003}$	$0.343^{+0.002}_{-0.002}$	$0.090^{+0.006}_{-0.004}$	$-0.261^{+0.000}_{-0.001}$	$30.8^{+4.0}_{-4.0}$
		QCDW	$0.333^{+0.003}_{-0.002}$	$0.327^{+0.001}_{-0.001}$	$0.065^{+0.006}_{-0.004}$	$-0.242^{+0.000}_{-0.001}$	$30.3^{+4.0}_{-4.0}$
		$\frac{\text{2HDM}}{\text{QCDW}}$ [%]	$5.41^{+0.17}_{-0.17}$	$4.97^{+0.10}_{-0.08}$	$38.4^{+4.0}_{-4.0}$	$8.18^{+0.26}_{-0.26}$	$1.57^{+0.12}_{-0.07}$

Table 13: *P*- and *CP*-even spin correlations and dileptonic cross section in scenario 1c for the LHC(13 TeV).

			C_{hel}	C_{nn}	C_{rr}	D	$\sigma_{t\bar{t}}$×BR [pb]
$2m_t \leq M_{t\bar{t}} \leq 400$ GeV	LO	2HDM+QCD	$0.582^{+0.011}_{-0.011}$	$0.539^{+0.005}_{-0.005}$	$0.311^{+0.011}_{-0.010}$	$-0.477^{+0.009}_{-0.009}$	$3.75^{+0.90}_{-0.68}$
		QCD	$0.562^{+0.011}_{-0.011}$	$0.528^{+0.005}_{-0.005}$	$0.289^{+0.011}_{-0.011}$	$-0.459^{+0.009}_{-0.009}$	$3.58^{+0.85}_{-0.65}$
		$\frac{\text{2HDM}}{\text{QCD}}$ [%]	$3.51^{+0.12}_{-0.12}$	$2.21^{+0.05}_{-0.05}$	$7.78^{+0.38}_{-0.36}$	$3.91^{+0.13}_{-0.12}$	$4.73^{+0.06}_{-0.06}$
	NLO	2HDM+QCDW	$0.577^{+0.008}_{-0.010}$	$0.539^{+0.004}_{-0.005}$	$0.360^{+0.002}_{-0.002}$	$-0.492^{+0.005}_{-0.005}$	$6.42^{+0.87}_{-0.78}$
		QCDW	$0.548^{+0.009}_{-0.011}$	$0.522^{+0.004}_{-0.005}$	$0.330^{+0.003}_{-0.002}$	$-0.466^{+0.006}_{-0.005}$	$6.06^{+0.81}_{-0.73}$
		$\frac{\text{2HDM}}{\text{QCDW}}$ [%]	$5.18^{+0.29}_{-0.29}$	$3.32^{+0.10}_{-0.07}$	$9.24^{+0.22}_{-0.21}$	$5.45^{+0.21}_{-0.18}$	$5.93^{+0.27}_{-0.20}$
$400 \leq M_{t\bar{t}} \leq 460$ GeV	LO	2HDM+QCD	$0.408^{+0.009}_{-0.009}$	$0.337^{+0.002}_{-0.002}$	$0.013^{+0.006}_{-0.006}$	$-0.253^{+0.006}_{-0.006}$	$4.36^{+1.10}_{-0.83}$
		QCD	$0.432^{+0.009}_{-0.009}$	$0.356^{+0.002}_{-0.002}$	$0.045^{+0.006}_{-0.006}$	$-0.278^{+0.006}_{-0.006}$	$4.54^{+1.10}_{-0.87}$
		$\frac{\text{2HDM}}{\text{QCD}}$ [%]	$-5.41^{+0.15}_{-0.15}$	$-5.47^{+0.01}_{-0.01}$	$-71.7^{+9.0}_{-12.0}$	$-9.02^{+0.19}_{-0.20}$	$-3.95^{+0.03}_{-0.03}$
	NLO	2HDM+QCDW	$0.421^{+0.010}_{-0.010}$	$0.356^{+0.003}_{-0.002}$	$0.100^{+0.001}_{+0.000}$	$-0.293^{+0.004}_{-0.004}$	$7.36^{+0.95}_{-0.88}$
		QCDW	$0.426^{+0.007}_{-0.007}$	$0.362^{+0.001}_{-0.000}$	$0.107^{+0.004}_{-0.003}$	$-0.298^{+0.001}_{-0.001}$	$7.53^{+0.98}_{-0.91}$
		$\frac{\text{2HDM}}{\text{QCDW}}$ [%]	$-1.15^{+0.67}_{-0.74}$	$-1.65^{+0.55}_{-0.61}$	$-6.02^{+3.00}_{-3.00}$	$-1.91^{+0.88}_{-1.00}$	$-2.15^{+0.08}_{-0.09}$
incl. in $M_{t\bar{t}}$	LO	2HDM+QCD	$0.295^{+0.003}_{-0.004}$	$0.328^{+0.000}_{-0.001}$	$-0.019^{+0.002}_{-0.003}$	$-0.201^{+0.002}_{-0.002}$	$18.6^{+5.0}_{-4.0}$
		QCD	$0.297^{+0.003}_{-0.004}$	$0.329^{+0.000}_{-0.001}$	$-0.017^{+0.002}_{-0.003}$	$-0.203^{+0.002}_{-0.002}$	$18.6^{+5.0}_{-4.0}$
		$\frac{\text{2HDM}}{\text{QCD}}$ [%]	$-0.735^{+0.009}_{-0.013}$	$-0.294^{+0.006}_{-0.007}$	$12.0^{+2.0}_{-2.0}$	$-0.853^{+0.011}_{-0.015}$	$-0.310^{+0.010}_{-0.011}$
	NLO	2HDM+QCDW	$0.339^{+0.004}_{-0.003}$	$0.331^{+0.002}_{-0.001}$	$0.073^{+0.006}_{-0.004}$	$-0.248^{+0.000}_{-0.001}$	$30.5^{+4.0}_{-4.0}$
		QCDW	$0.333^{+0.003}_{-0.002}$	$0.327^{+0.001}_{-0.001}$	$0.065^{+0.006}_{-0.004}$	$-0.242^{+0.000}_{-0.001}$	$30.3^{+4.0}_{-4.0}$
		$\frac{\text{2HDM}}{\text{QCDW}}$ [%]	$2.01^{+0.16}_{-0.17}$	$1.21^{+0.09}_{-0.09}$	$11.4^{+2.0}_{-2.0}$	$2.49^{+0.20}_{-0.21}$	$0.442^{+0.033}_{-0.017}$

Table 14: *P*- and *CP*-even spin correlations and dileptonic cross section in scenario 2 for the LHC(13 TeV).

			C_{hel}	C_{nn}	C_{rr}	D	$\sigma_{t\bar{t}}\times$BR [pb]
$670 \leq M_{t\bar{t}} \leq 770$ GeV	LO	2HDM+QCD	$0.012^{+0.006}_{-0.006}$	$0.217^{+0.001}_{-0.001}$	$-0.217^{+0.003}_{-0.003}$	$-0.004^{+0.003}_{-0.003}$	$1.16^{+0.35}_{-0.25}$
		QCD	$0.021^{+0.006}_{-0.006}$	$0.226^{+0.001}_{-0.001}$	$-0.204^{+0.003}_{-0.003}$	$-0.014^{+0.003}_{-0.003}$	$1.17^{+0.35}_{-0.25}$
		$\frac{\text{2HDM}}{\text{QCD}}$ [%]	$-42.9^{+10.0}_{-18.0}$	$-3.95^{+0.05}_{-0.06}$	$6.28^{+0.14}_{-0.12}$	$-72.4^{+11.0}_{-16.0}$	$-0.899^{+0.010}_{-0.011}$
	NLO	2HDM+QCDW	$0.125^{+0.011}_{-0.012}$	$0.198^{+0.004}_{-0.004}$	$-0.103^{+0.000}_{-0.001}$	$-0.072^{+0.005}_{-0.005}$	$1.91^{+0.25}_{-0.25}$
		QCDW	$0.103^{+0.001}_{-0.000}$	$0.201^{+0.002}_{-0.002}$	$-0.110^{+0.008}_{-0.007}$	$-0.063^{+0.002}_{-0.003}$	$1.90^{+0.26}_{-0.25}$
		$\frac{\text{2HDM}}{\text{QCDW}}$ [%]	$21.8^{+11.0}_{-12.0}$	$-1.34^{+0.81}_{-1.00}$	$-6.95^{+6.80}_{-5.10}$	$14.3^{+11.0}_{-12.0}$	$0.953^{+0.433}_{-0.628}$
$770 \leq M_{t\bar{t}} \leq 870$ GeV	LO	2HDM+QCD	$-0.083^{+0.006}_{-0.006}$	$0.232^{+0.001}_{-0.001}$	$-0.215^{+0.003}_{-0.003}$	$0.022^{+0.002}_{-0.002}$	$0.622^{+0.194}_{-0.139}$
		QCD	$-0.067^{+0.006}_{-0.006}$	$0.223^{+0.001}_{-0.001}$	$-0.217^{+0.003}_{-0.003}$	$0.020^{+0.002}_{-0.002}$	$0.631^{+0.197}_{-0.141}$
		$\frac{\text{2HDM}}{\text{QCD}}$ [%]	$25.2^{+2.0}_{-2.0}$	$4.04^{+0.04}_{-0.04}$	$-0.956^{+0.036}_{-0.039}$	$9.42^{+1.10}_{-0.88}$	$-1.55^{+0.01}_{-0.01}$
	NLO	2HDM+QCDW	$0.032^{+0.009}_{-0.007}$	$0.185^{0.000}_{-0.001}$	$-0.117^{+0.015}_{-0.010}$	$-0.034^{+0.007}_{-0.007}$	$1.01^{+0.15}_{-0.14}$
		QCDW	$0.041^{+0.004}_{-0.003}$	$0.185^{+0.002}_{-0.004}$	$-0.115^{+0.010}_{-0.006}$	$-0.037^{+0.003}_{-0.003}$	$1.02^{+0.15}_{-0.14}$
		$\frac{\text{2HDM}}{\text{QCDW}}$ [%]	$-21.7^{+13.0}_{-13.0}$	$0.279^{+1.460}_{-1.250}$	$1.52^{+3.40}_{-4.60}$	$-9.13^{+11.00}_{-12.00}$	$-1.20^{+0.37}_{-0.26}$
incl. in $M_{t\bar{t}}$	LO	2HDM+QCD	$0.298^{+0.003}_{-0.004}$	$0.329^{+0.000}_{-0.000}$	$-0.016^{+0.002}_{-0.003}$	$-0.204^{+0.002}_{-0.002}$	$17.8^{+5.0}_{-4.0}$
		QCD	$0.296^{+0.004}_{-0.004}$	$0.329^{+0.000}_{-0.000}$	$-0.018^{+0.002}_{-0.003}$	$-0.203^{+0.002}_{-0.002}$	$17.7^{+5.0}_{-4.0}$
		$\frac{\text{2HDM}}{\text{QCD}}$ [%]	$0.589^{+0.019}_{-0.019}$	$0.061^{+0.003}_{-0.004}$	$-6.05^{+0.66}_{-0.71}$	$0.494^{+0.017}_{-0.018}$	$0.249^{+0.003}_{-0.004}$
	NLO	2HDM+QCDW	$0.337^{+0.004}_{-0.003}$	$0.328^{+0.002}_{-0.001}$	$0.066^{+0.005}_{-0.004}$	$-0.244^{+0.000}_{-0.001}$	$29.6^{+4.0}_{-4.0}$
		QCDW	$0.333^{+0.004}_{-0.002}$	$0.327^{+0.002}_{-0.001}$	$0.064^{+0.006}_{-0.004}$	$-0.242^{+0.000}_{-0.001}$	$29.5^{+4.0}_{-4.0}$
		$\frac{\text{2HDM}}{\text{QCDW}}$ [%]	$1.08^{+0.10}_{-0.12}$	$0.159^{+0.022}_{-0.026}$	$3.38^{+0.69}_{-0.74}$	$0.867^{+0.100}_{-0.119}$	$0.421^{+0.016}_{-0.023}$

References

[1] ATLAS Collaboration, G. Aad et al., *Observation of a new particle in the search for the Standard Model Higgs boson with the ATLAS detector at the LHC*, Phys. Lett. **B716** (2012) 1–29, arXiv:1207.7214 [hep-ex].

[2] CMS Collaboration, S. Chatrchyan et al., *Observation of a new boson at a mass of 125 GeV with the CMS experiment at the LHC*, Phys. Lett. **B716** (2012) 30–61, arXiv:1207.7235 [hep-ex].

[3] A. Djouadi, *The Anatomy of electro-weak symmetry breaking. II. The Higgs bosons in the minimal supersymmetric model*, Phys. Rept. **459** (2008) 1–241, arXiv:hep-ph/0503173 [hep-ph].

[4] G. C. Branco, P. M. Ferreira, L. Lavoura, M. N. Rebelo, M. Sher, and J. P. Silva, *Theory and phenomenology of two-Higgs-doublet models*, Phys. Rept. **516** (2012) 1–102, arXiv:1106.0034 [hep-ph].

[5] F. Canelli, *Recent results from Higgs physics at the LHC*, plenary talk given at ICHEP, Chicago, 2016.

[6] CMS Collaboration, S. Chatrchyan et al., *Searches for new physics using the $t\bar{t}$ invariant mass distribution in pp collisions at $\sqrt{s} = 8$ TeV*, Phys. Rev. Lett. **111** no. 21, (2013) 211804, arXiv:1309.2030 [hep-ex]. [Erratum: Phys. Rev. Lett.112,no.11,119903(2014)].

[7] ATLAS Collaboration, G. Aad et al., *A search for $t\bar{t}$ resonances using lepton-plus-jets events in proton-proton collisions at $\sqrt{s} = 8$ TeV with the ATLAS detector*, JHEP **08** (2015) 148, arXiv:1505.07018 [hep-ex].

[8] CMS Collaboration, V. Khachatryan et al., *Search for resonant $t\bar{t}$ production in proton-proton collisions at $\sqrt{s} = 8$ TeV*, Phys. Rev. **D93** no. 1, (2016) 012001, arXiv:1506.03062 [hep-ex].

[9] ATLAS collaboration, *Search for heavy Higgs bosons A/H decaying to a top-quark pair in pp collisions at $\sqrt{s} = 8$ TeV with the ATLAS detector*, ATLAS-CONF-2016-073.

[10] W. Bernreuther, P. Galler, C. Mellein, Z. G. Si, and P. Uwer, *Production of heavy Higgs bosons and decay into top quarks at the LHC*, Phys. Rev. **D93** no. 3, (2016) 034032, arXiv:1511.05584 [hep-ph].

[11] B. Hespel, F. Maltoni, and E. Vryonidou, *Signal background interference effects in heavy scalar production and decay to a top-anti-top pair*, JHEP **10** (2016) 016, arXiv:1606.04149 [hep-ph].

[12] W. Bernreuther, A. Brandenburg, Z. G. Si, and P. Uwer, *Top quark pair production and decay at hadron colliders*, Nucl. Phys. **B690** (2004) 81–137, arXiv:hep-ph/0403035 [hep-ph].

[13] W. Bernreuther, D. Heisler, and Z.-G. Si, *A set of top quark spin correlation and polarization observables for the LHC: Standard Model predictions and new physics contributions*, JHEP **12** (2015) 026, arXiv:1508.05271 [hep-ph].

[14] W. Bernreuther and A. Brandenburg, *Tracing CP violation in the production of top quark pairs by multiple TeV proton proton collisions*, Phys. Rev. **D49** (1994) 4481–4492, arXiv:hep-ph/9312210 [hep-ph].

[15] W. Bernreuther, M. Flesch, and P. Haberl, *Signatures of Higgs bosons in the top quark decay channel at hadron colliders*, Phys. Rev. **D58** (1998) 114031, arXiv:hep-ph/9709284 [hep-ph].

[16] W. Bernreuther, A. Brandenburg, and M. Flesch, *Effects of Higgs sector CP violation in top quark pair production at the LHC*, arXiv:hep-ph/9812387 [hep-ph].

[17] M. Baumgart and B. Tweedie, *Discriminating Top-Antitop Resonances using Azimuthal Decay Correlations*, JHEP **09** (2011) 049, arXiv:1104.2043 [hep-ph].

[18] V. Barger, W.-Y. Keung, and B. Yencho, *Azimuthal Correlations in Top Pair Decays and The Effects of New Heavy Scalars*, Phys. Rev. **D85** (2012) 034016, arXiv:1112.5173 [hep-ph].

[19] C.-Y. Chen, S. Dawson, and Y. Zhang, *Complementarity of LHC and EDMs for Exploring Higgs CP Violation*, JHEP **06** (2015) 056, arXiv:1503.01114 [hep-ph].

[20] C. Mellein, *Production of heavy Higgs bosons and decay into top quarks at the LHC*. PhD thesis. Rheinisch-Westfälische Technische Hochschule (RWTH) Aachen, 2015.

[21] ATLAS, CMS Collaboration, G. Aad et al., *Measurements of the Higgs boson production and decay rates and constraints on its couplings from a combined ATLAS and CMS analysis of the LHC pp collision data at* $\sqrt{s} = 7$ *and 8 TeV*, JHEP **08** (2016) 045, arXiv:1606.02266 [hep-ex].

[22] E. Braaten and J. P. Leveille, *Higgs Boson Decay and the Running Mass*, Phys. Rev. **D22** (1980) 715.

[23] M. Drees and K.-i. Hikasa, *Note on QCD corrections to hadronic Higgs decay*, Phys. Lett. **B240** (1990) 455. [Erratum: Phys. Lett.B262,497(1991)].

[24] M. Spira, A. Djouadi, D. Graudenz, and P. M. Zerwas, *Higgs boson production at the LHC*, Nucl. Phys. **B453** (1995) 17–82, arXiv:hep-ph/9504378 [hep-ph].

[25] A. Djouadi, J. Kalinowski, and M. Spira, *HDECAY: A Program for Higgs boson decays in the standard model and its supersymmetric extension*, Comput. Phys. Commun. **108** (1998) 56–74, arXiv:hep-ph/9704448 [hep-ph].

[26] D. Eriksson, J. Rathsman, and O. Stal, *2HDMC: Two-Higgs-Doublet Model Calculator Physics and Manual*, Comput. Phys. Commun. **181** (2010) 189–205, arXiv:0902.0851 [hep-ph].

[27] F. Mahmoudi and O. Stal, *Flavor constraints on the two-Higgs-doublet model with general Yukawa couplings*, Phys. Rev. **D81** (2010) 035016, arXiv:0907.1791 [hep-ph].

[28] T. Hermann, M. Misiak, and M. Steinhauser, *$\bar{B} \to X_s\gamma$ in the Two Higgs Doublet Model up to Next-to-Next-to-Leading Order in QCD*, JHEP **11** (2012) 036, arXiv:1208.2788 [hep-ph].

[29] O. Eberhardt, U. Nierste, and M. Wiebusch, *Status of the two-Higgs-doublet model of type II*, JHEP **07** (2013) 118, arXiv:1305.1649 [hep-ph].

[30] A. Kobakhidze, N. Liu, L. Wu, and J. Yue, *Implications of CP-violating Top-Higgs Couplings at LHC and Higgs Factories*, arXiv:1610.06676 [hep-ph].

[31] CMS Collaboration, V. Khachatryan et al., *Search for CP violation in top quark-antiquark production and decay in proton-proton collisions at $\sqrt{s} = 8$ TeV*, Submitted to: JHEP (2016) , arXiv:1611.08931 [hep-ex].

[32] ATLAS Collaboration, M. Aaboud et al., *Measurements of top quark spin observables in $t\bar{t}$ events using dilepton final states in $\sqrt{s} = 8$ TeV pp collisions with the ATLAS detector*, arXiv:1612.07004 [hep-ex].

[33] S. Inoue, M. J. Ramsey-Musolf, and Y. Zhang, *CP-violating phenomenology of flavor conserving two Higgs doublet models*, Phys. Rev. **D89** no. 11, (2014) 115023, arXiv:1403.4257 [hep-ph].

[34] V. Cirigliano, W. Dekens, J. de Vries, and E. Mereghetti, *Constraining the top-Higgs sector of the Standard Model Effective Field Theory*, Phys. Rev. **D94** no. 3, (2016) 034031, arXiv:1605.04311 [hep-ph].

[35] V. Cirigliano, W. Dekens, J. de Vries, and E. Mereghetti, *Is there room for CP violation in the top-Higgs sector?*, Phys. Rev. **D94** no. 1, (2016) 016002, arXiv:1603.03049 [hep-ph].

[36] C. A. Baker et al., *An Improved experimental limit on the electric dipole moment of the neutron*, Phys. Rev. Lett. **97** (2006) 131801, arXiv:hep-ex/0602020 [hep-ex].

[37] ACME Collaboration, J. Baron et al., *Order of Magnitude Smaller Limit on the Electric Dipole Moment of the Electron*, Science **343** (2014) 269–272, arXiv:1310.7534 [physics.atom-ph].

[38] A. Czarnecki, M. Jezabek, and J. H. Kuhn, *Lepton Spectra From Decays of Polarized Top Quarks*, Nucl. Phys. **B351** (1991) 70–80.

[39] S. Berge, W. Bernreuther, and S. Kirchner, *Determination of the Higgs CP-mixing angle in the tau decay channels at the LHC including the DrellYan background*, Eur. Phys. J. **C74** no. 11, (2014) 3164, arXiv:1408.0798 [hep-ph].

[40] H.-L. Lai, M. Guzzi, J. Huston, Z. Li, P. M. Nadolsky, J. Pumplin, and C. P. Yuan, *New*

parton distributions for collider physics, Phys. Rev. **D82** (2010) 074024, arXiv:1007.2241 [hep-ph].

[41] LHC Higgs Cross Section Working Group Collaboration, S. Dittmaier et al., *Handbook of LHC Higgs Cross Sections: 1. Inclusive Observables*, arXiv:1101.0593 [hep-ph].

[42] A. Djouadi, J. Ellis, and J. Quevillon, *Interference effects in the decays of spin-zero resonances into $\gamma\gamma$ and $t\bar{t}$*, JHEP **07** (2016) 105, arXiv:1605.00542 [hep-ph].

[43] CMS Collaboration, V. Khachatryan et al., *Measurements of t t-bar spin correlations and top quark polarization using dilepton final states in pp collisions at sqrt(s) = 8 TeV*, Phys. Rev. **D93** no. 5, (2016) 052007, arXiv:1601.01107 [hep-ex].